MAPPING CARBON STOCK IN TREES OUTSIDE FOREST: COMPARING A VERY HIGH RESOLUTION OPTICAL SATELLITE IMAGE (GEO-EYE) AND AIRBORNE LIDAR DATA IN CHITWAN, NEPAL

ITOE CONSTANTINE NFOR NGWAYI
Enschede, The Netherlands, February, 2012

SUPERVISORS:
Drs. E. Henk Kloosterman
Dr. Ir. Thomas Groen

MAPPING CARBON STOCK IN TREES OUTSIDE FOREST: COMPARING VERY HIGH RESOLUTION OPTICAL SATELLITE IMAGE (GEO-EYE) AND AIRBORNE LIDAR DATA IN CHITWAN, NEPAL

ITOE CONSTANTINE NFOR NGWAYI
Enschede, The Netherlands, February, 2012

Thesis submitted to the Faculty of Geo-Information Science and Earth Observation of the University of Twente in partial fulfilment of the requirements for the degree of Master of Science in Geo-information Science and Earth Observation.
Specialization: Natural Resource Management

SUPERVISORS:
Drs. E. Henk Kloosterman
Dr. Ir. Thomas Groen

THESIS ASSESSMENT BOARD:
Dr. Y. A. Hussin (Chair)
Dr. T. Kauranne (External Examiner),
Arbonaut Oy Ltd and Dept. of Mathematics & Physics, Lappeenranta University of Technology, Finland

ABSTRACT

In this study, object based image analysis (OBIA) was used to compare the segmentation accuracy for trees outside forest (ToF) using a VHR Geo-Eye satellite image and airborne LiDAR data in mapping carbon stock. While CPA that is a proxy for DBH was used for the Geo-Eye, CPA and canopy height model (CHM) was used for the airborne LiDAR data from which a multiple regression analysis was applied.

DBH was randomly measured from all the available trees in the field alongside the tree height and the crown diameter. Quantification of AGB was estimated with the use of a mixed allometric equation for tropical forest described in Chave et al., (2005). Regression equations were developed between the field measured parameters, field measured DBH and remote sensing parameters and the result indicated that the coefficient of determination, $R^2>0.5$.

The accuracy assessment result of the segmentation process was 79% and 74% for the airborne LiDAR data and Geo-Eye respectively. The result of the relationship between the field measured and that of remotely sensed data was $R^2=0.74$ (RMSE=38.24%) and $R^2=0.73$ (RMSE=41.18%) respectively for the LiDAR and Geo-Eye data sets. The highest quantity of predicted carbon was from the airborne LiDAR data that had an R^2 of 0.90 and RMSE of 14.24%. However, the best model is from the multiple regression of the LiDAR data parameters of CHM and CPA with $R^2=0.69$ (RMSE=11.53%). The predicted carbon of the Geo-Eye had $R^2=0.51$ with 42.24% RMSE. The result of OBIA gives airborne LiDAR an edge to Geo-Eye image in estimating CPA due to her 3-D characteristic in determining forest structures. The *t-test* result rejected the null hypothesis that there was a significant difference between the segmented CPAs of the two data sets at 95% confidence interval.

The major problem of this study was the identification of pruned tree crowns on the Geo-Eye image. Further investigation should be carried out with a stratified random sampling of the crown size to uniformly distribute the data set of the study. These findings will be useful to the CFUGs and the Forestry Department of Nepal to propose integration of ToF into their natural resource management scheme for carbon stock estimation. Nevertheless, this study encourages the use of airborne LiDAR data for carbon stock estimation for trees outside forest in a tropical environment like Nepal.

Keywords: aboveground carbon stock, OBIA, trees outside forest, Geo-Eye, LiDAR, tree height, crown projection area, Nepal.

ACKNOWLEDGEMENTS

Like a sculpture, this piece of work is the fruit of months of moulding with skills and determination. However, it would not have been possible without the support of many individuals and Organisations. My sincere gratitude goes to the Joint Japan/ World Bank Graduate Scholarship Program for financing my studies at the Faculty of Geo-Information Science and Earth Observation (ITC) and the Government of Cameroon for granting me a study leave.

Firstly, I am heartily thankful to my supervisor, Drs. E. Henk Kloosterman who gave me his unflinching encouragement, guidance and support through my thesis period. His detailed and constructive comments produced the foundation of this thesis. Many thanks also go to Dr. Thomas Groen whose ideas and suggestions made the work more stimulating as my second supervisor.

I am thankful to ITC for facilitating my studies and research and most particularly to the NRM staffs who contributed enormously in transferring the skills of GIS and Remote Sensing to us. Here, I am grateful to the Carbon and Climate Change group leader Dr. Y. A. Hussin for his fatherly encouragement and field assistance and the Course Director, Dr. M. J. C. Weir for his critical comments during the proposal and mid-term evaluation phases.

My deep appreciation goes to the ICIMOD Project, most especially Hammad Gilani for providing the necessary data and facilitating our fieldwork in Nepal, Forest Resource Assessment (FRA), Federation of Community Forest Users' Nepal (FECOFUN), Asian Network for Sustainable Agriculture and Bio-resources (ANSAB) and the Community of Chitwan for their hospitality. Special thanks to Basanta Gautam of Arbonaut and Khamarrul A. Razak (*Ph.D student at ITC*) for providing an insight on the use of LiDAR data. My thankfulness goes to my field guides Bimal Rayamajhi, Jay Bhattarai and Kamal Khadka who did their work diligently with lots of determination during the data collection campaign. I would also wish to express my heart-felt gratitude to my field group mates Amado Lopez, Olusola Adefurin, Purity Mbaabu and Yogendra Karna with whom I shared the tough and cheerful moments.

My colleagues of the Department of NRM have contributed enormously to my personal and professional development. Your smiles within the corridors cooled my brains in challenging times and I appreciate the ideas we shared within the multi-cultural environment.

Finally, my deepest gratitude goes to my family most especially my wife, Elema Alma, my friends and the youths of Kake (II) Bokoko village for all their strength and moral support throughout my studies.

This piece of work is dedicated to my mother, Mrs Bertha Ngonde Ndome ep. NGANDA, r the ultimate source of my inspiration!!!

TABLE OF CONTENTS

LIST OF FIGURES

LIST OF TABLES

ACRONYMS

AGB	Above ground biomass
ANOVA	Analysis of variance
ANSAB	Asian Network of Sustainable Agriculture and Bio-resources
CF	Community Forest
CFUG	Community Forests User Groups
CO_2	Carbondioxide
CPA	Crown Projection Area
DBH	Diameter at Breast Height
DEM	Digital Elevation Model
DN	Digital number
FECOFUN	Federation of Community Forest Users' Nepal
GHGs	Greenhouse gases
GIS	Geographic Information System
GPS	Global positioning system
HPF	high pass filter
ICIMOD	International Centre for Integrated Mountain Development
IHS	Intensity hue saturation
IPCC	Intergovernmental Panel on Climate Change
JTS	Java Topology Suite
LiDAR	Light Detection and Ranging
MSS	multispectral data
NDVI	Normalised Difference Vegetation Index
OBIA	Object-based image analysis
REDD	Reduction Emission from Deforestation and Forest Degradation
RGB	Red, Green and Blue
SWD	specific wood density
UNFCCC	United Nations Framework Convention on Climate Change
VHR	Very high resolution

1. INTRODUCTION

1.1. Background

The forests of the world constitute about 31% of the total land area just over 4 billion hectares (FAO, 2010). The forest stores more than 650 billion tonnes of organic carbon in both trees and soil of which 44% is in biomass (FAO, 2010). Compared to other ecosystems, forests are known to play an important role in the global carbon (C) cycle as it influences the climate and climate change processes; and are globally cherished for numerous services to the society (Pan *et al.*, 2011). Most importantly, the forest serves as a brake through to climatic variations due to its ability in carbon sequestration and storage (Gibbs *et al.*, 2007). However, forests absorb carbon in wood, leaves and organic matter and release it into the atmosphere during the deforestation processes (e.g. burning and clearing of land) (FAO, 2010) leading to carbondioxide (CO_2) emission. Quantification of large forest carbon stocks is imperative for national inventories for net greenhouse gas (GHG) emissions (Wang *et al.*, 2007) and to verify the function of terrestrial carbon storage in the global carbon cycle.

The Intergovernmental Panel on Climate Change (IPCC) predicted a rise in the world's temperature by the end of the century from 1.8°C to 4°C due to an increase in the concentration of the amount of GHGs from anthropogenic factors (IPCC, 2007). These GHGs are emitted through the fossil fuel combustion and forest cover changes resulting from other land uses. This dynamics of forest degradation remains inadequately understood (Houghton *et al.*, 1992) as the value of mature and secondary tropical forest as sinks of atmospheric CO_2 are less considered in carbon stock estimations (Lugo & Brown, 1986). Terrestrial forest ecosystems of low and mid-altitude was proposed to be significantly responsible for the imbalance in the carbon budget (Tan *et al.*, 1990) as this zone is highly affected by anthropogenic activities. To mitigate on the anticipated temperature rise by the end of the Century, the Bali Action Plan of the United Nations Framework Convention on Climate Change (UNFCCC) in 2007 introduced a policy of "*Reducing emissions from Deforestation and Forest Degradation*" mechanism within the developing countries (UN-REDD, 2008) to implement the Kyoto Protocol treaty that was initiated in December 1997 and came into force in February 16th, 2005.

Forest biomass assessment is important for national development planning as well as for scientific studies of ecosystem productivity and carbon budgets. Typically, carbon stock is obtained from above-ground biomass (AGB) as 50% of tree biomass is made up of carbon (Basuki *et al.*, 2009). Estimation of biomass of forests is a usual practice to quantify fuel and wood stock and allocate harvestable amount. Traditionally, the most accurate method for biomass estimation is through felling of trees and weighing of their parts with a scale (Basuki, *et al.*, 2009). This method is destructive, requires much time, heavy manpower and is not profitable for large geographic coverage (Popescu, 2007; Verwijst & Telenius, 1999). Nonetheless, the method is used for validation of less aggressive and expensive methods like using remotely sensed data for carbon stock estimation (Wang *et al.*, 2003). Methods of data collection range from satellite imagery to aerial photo-imagery obtained from low flying planes (Brown, 2002).

Even though remotely sensed data are a proxy for AGB, the fact that they provide consistent quantitative data over large areas, makes remote sensing based carbon stock mapping far superior to extrapolations based on field measurements (Popescu, 2007) as there is no remote-sensing instrument that is capable to

measure forest carbon stock directly (Drake *et al.*, 2003). The advantages of using remote sensing in biomass estimation include the possibility to obtain measurements from every location of the forest, the speed of data collection and processing, the relatively low cost of many remote sensing data types, and the ability to easily collect data from difficult to access ground terrains (Bortolot & Wynne, 2005).

There is high inconsistency in the accuracy to obtain AGB from optical data and this varies with the different case studies and methods in application (Holmgren & Thuresson, 1998; Wulder, 1998). Optical sensors provide systematic observations at regional/global and at coarse (>1 km) spatial resolution (Rosenqvist *et al.*, 2003). Their frequencies of occurrence stretch from several times daily (e.g. NOAA AVHRR) to every 16-18 days (e.g. Landsat ETM+) that makes the data prune to haze, smoke and most especially cloud cover in the tropics. Generally, there is a weak relationship between carbon stock and field-based measurements from optical sensors in estimating forest biomass predictions from satellite-observed vegetation indices (Foody *et al.*, 2003). Biomass data from optical sensors are often inaccurate and generally insufficient to estimate carbon stocks of various vegetation types alone (Rosenqvist, *et al.*, 2003). Remote-sensing systems are restricted by haze, smoke and most especially cloud cover in the tropics, although modern technologies including radar systems can penetrate clouds to obtain day and night data.

In comparison to the use of optical remote sensing, there has been a great success in the application of remote-sensing techniques to estimate carbon stocks from airborne LiDAR in boreal and temperate forests. "LiDAR collects samples along the flight path and as such, is not an imaging system" (Patenaude et al., 2005). The level of estimated uncertainties of carbon stock is reduced and range between 10-15% in temperate forests (Lefsky *et al.*, 2002a; Popescu *et al.*, 2004). Unfortunately, the range of uncertainty tropical forest is vast (8-25%) promoted by the topography (Drake, *et al.*, 2003) although they are characterise to be among the richest ecosystem in carbon content (Asner, 2009).

The use of airborne Light Detection and Ranging (LiDAR) data to estimate forest stand tree height has gained widespread attention (Lim *et al.*, 2003; Naesset, 1997). The point cloud density of LiDAR data is delivered in X, Y and Z (3-D) format from which the structural parameters of tree height and CPA can be estimated. Interpolation involving tree structural samples is essential for thematic mapping (Patenaude, et al., 2005) as relationships can be established to estimate forest carbon stock though tropical forest quickly attain maximum height and continue to accumulate carbon for many decades (Hese *et al.*, 2005). The extensive coverage of LiDAR remote sensing overrides the proficiencies of radar and optical sensors to estimate carbon stocks for all forest types (Drake, et al., 2003; Lefsky, et al., 2002a).

In spite of the advantages of LiDAR, LiDAR would probably be too costly for monitoring a larger forest area. Hence, a sampling approach is applied for a subset which is later extended to the whole region (Gibbs *et al.*, 2007; Wulder & Seemann, 2003). The lack of collective algorithmic standards or unavailability of published processing algorithms like all remotely sensed data makes the application of LiDAR data difficult. But its 3-dimensional structure of data acquisition makes it more adaptable. Similarly, the estimation of stand height from LiDAR data would be highly dependent on the terrain, slope angle and the canopy cover of the vegetation (Gatziolis *et al.*, 2010). LiDAR's limitation as most remotely sensed data is the indiscriminate distinction of tree species as biomass varies between tree species of similar height and age using allometric equations (Rosenqvist, et al., 2003). However, incorporation of Lidar with hyper-spectral data from which tree species can be identified, may allow biomass to be estimated with more accuracy (Lu, 2006).

Using VHR Satellite imagery, it is possible to obtain the crown projection area (CPA) or a segment of the trees with the help of object-based image analysis (OBIA) technique. Experimental results have shown field measured CPA and DBH to be highly correlated (Hemery *et al.*, 2005) and therefore can be employed for forest biomass studies (Alves & Santos, 2002). Direct field measurement of CPA is time consuming rendering its application rare (Song, 2007) thereby promoting researchers to an alternative use of OBIA to estimate CPA effectively over a wide region. Li & Strahler, (1985) modelled the estimation of CPA from satellite imagery using Landsat TM with some success but unfortunately, using the Li-Strahler model, there was difficulty in separating the individual tree crowns from the canopy cover with Landsat TM imagery (Woodcock *et al.*, 1997). Alternatively, the introduction of OBIA that has been successfully identified and applied for CPA delineation using VHR multispectral imagery (Kim *et al.*, 2009).

The two processes of image segmentation for individual tree crown delineation are i) Individual Tree Crown (ITC) algorithm (Gougeon, 1995) that is an extension of the image processing software PCI Geomatica (Mora *et al.*, 2010) and ii) OBIA software called eCognition Developper8 (Kim, *et al.*, 2009). Some studies have demonstrated the successes in the application of the ITC algorithm on series of imageries and different forest situations (Gougeon *et al.*, 2003; Leckie *et al.*, 2003). The ITC technique is based on differentiation of either the tree crown or its shadow.

Likewise, the eCognition 8 (or Definiens Developer) that has been gaining much credence recently is characterised by the delineation of the individual tree crowns (image object segments) and tree species classification (Benz *et al.*, 2004). "Generation of a segment is dependent on one or more homogeneity criteria in one or more spatial dimensions (distances, neighbourhoods, topologies etc.) of the feature space" (Blaschke, 2010). The scale parameter that determines the maximum extent of heterogeneity of the resulting image is dependent on the user as it is practically a trial and error approach since no automatic or objective specific method exists (Hay *et al.*, 2003). Significant results of CPA delineation obtained from OBIA approach have been applied in different research work (Chubey et al., 2006; Pascual et al., 2008) and also for classification of trees outside the forest (Herrera, 2003). No matter how advanced the OBIA analysis, field data for validation are often required since "no single sensor on any satellite mission, whether Radar, LiDAR or optical, can be expected to provide consistently infallible estimates of biomass" (Goetz *et al.*, 2009).

1.2. Problem statement

In response to the UNFCCC and the Kyoto protocol on global climate change scenarios, periodic national inventories of GHG emissions and removals, as well as forest carbon inventories have to be reported annually (Patenaude *et al.*, 2005). The emerging global carbon markets that have integrated the Clean Development Mechanism (CDM) within the Kyoto Protocol need accurate and reliable techniques to compute sources and sinks of forest carbon. Presently, REDD proposition requires a valid and robust methodology to institute standard scenarios to estimate AGB carbon stock using remotely sensed data with high accuracy and extensive geographic coverage. This will institute annual monitoring with exact benefits sharing through payment for ecosystem services. This implies studies should be extended to involve Community-managed forests, Government-managed forests, trees outside forest (ToF) and other categories of forest types across the countries that ratified the COP 15 to determine their carbon stock potential.

A quantitative assessment of remote-sensing approaches for AGB carbon stock estimation proposed a synergetic use of approaches to override the limitations of each sensor such as Radar saturation, LiDAR sampling modes or optical temporal discrepancies (Goetz, *et al.*, 2009; Patenaude, *et al.*, 2005). A

combination of airborne LiDAR and multispectral data in a boreal forest gave an increase accuracy of adjusted R^2 of between 1 and 4% depending on species group (Hyyppa *et al.*, 2001) though closed canopy forest has overlapping crowns and are site-specific (Drake, *et al.*, 2003). Policy makers and planners are recognising trees inside and outside forests are diverse entities with mutual and synergetic potentials (Herrera, 2003). ToFs formulate an incredible supply of fodder, fuel wood, timber and fruits in Nepal (Weidner, 2008). But unfortunately, unlike trees inside forest, studies of the quantification and contribution of ToF of the tropics in the carbon cycle is scarce (Blaschke, 2010) though they serve as "leakages". There is a necessity to define and comprehend the underlying forces of ToF and their relation to carbon storage dynamics. Moreover, this would eventually result to a proper understanding of the value of ToF and their ultimate integration within sustainable management of Natural resources of forest, farm, pastoral and urban land.

The estimation of remote sensing based AGB carbon stock in the tropics remains a thought-provoking mission for researchers due to the complex nature of the biophysical environments (Lu, 2005). Most of the method developed from remotely sensed data is based on forest stand plantations. Species-specific regression models is impractical in tropics (Brown & Schroeder, 1999) as a 1-hectare plot may constitute more than 300 tree species with few occurrence (Gentry, 1988). Hence, biomass regression models for mixed tree species must be employed (Chave *et al.*, 2005).

This study aims to further develop and to improve on a method (Chave, et al., 2005) to assess carbon stock using CPA derived from VHR satellite image and airborne LiDAR data through object-based image analysis (OBIA), tree height from LiDAR data and forest stand parameters measured in the field for trees outside forest of Chitwan, Nepal. The Kayarkhola watershed is one of the selected pilot sites for the REDD+ implementation initiative by the UNFCCC in Nepal. The use of the above data is to obtain an accurate, precise and robust estimation for a sustainable monitoring development mechanism for Nepal (Gautam & Kandel, 2010).

1.3. Research objectives

The main objective of the study is to estimate and map carbon stock from individual trees using very high resolution (VHR) satellite image (Geo-Eye) and airborne LiDAR data for trees outside forest of Chitwan, Nepal.

1.3.1. Specific Objectives

- To assess the accuracy of segmentation technique for delineating individual crowns (CPA) of trees outside forest using VHR Geo-Eye satellite image and airborne LiDAR data.
- To assess the relationship between forest stand parameters from remotely sensed data (i.e. CPA and height) and field data.
- To estimate and map carbon accurately for trees outside forest in Kayarkhola watershed in Chitwan, Nepal.

1.3.2. Research Questions

- What is the difference in accuracy segmenting using VHR Geo-eye satellite image and airborne LiDAR data for trees outside forest?

- How strong is the relationship between forest stand parameters i.e. CPA and height extracted from remotely sensed data and field data for individual trees outside forest?
- What is the quantity of carbon stock in trees outside forest in the Kayarkhola watershed, Nepal?

Table 1: Objectives, research questions and hypotheses

Obj.	Research questions	Research Hypothesis
1	Can object-based image segmentation delineate individual tree crown with high accuracy from Geo-Eye and airborne Lidar data?	**H_0**: There is no significant difference in accuracy between the two data types using OBIA for tree crown delineation in trees outside forest. **H_1**: There is a significant difference between the two data types of delineation.
2	How strong is the relationship between CPA & tree height and carbon content?	**H_0**: There is no significant relationship between CPA & tree height and carbon of individual tree crowns **H_1**: There is a significant relationship between CPA & tree height and carbon of individual tree crowns
3	What is the quantity of carbon in the area?	

1.4. Definition of concepts

1.4.1. Forests

According to FAO, "these are lands of more than 0.5 hectares (ha), with tree canopy cover greater than 10%, which are primarily not under agriculture or urban land use. These trees should be able to reach a maximum height of 5m in-situ at maturity (FAO, 2002)". However, there is tolerance for each country to modify the definition depending on her course and her National Forestry Law. In this light, Nepal just like the FAO used 10% tree canopy cover as forest in their definition (Weidner, 2008).

1.4.2. Trees outside forest (ToF)

Though there exists no direct definition of trees outside forest (a neologism coined in 1995), FAO defines it as "trees growing outside the forest and not belonging to the category of forest, forest land, or other wooded land (FAO, 2002)". Some examples include:

a) Group of trees growing on an area of less than 0.5ha, including lines and shelter belts along infrastructure features and agricultural fields.

b) Scattered trees in agricultural landscapes.

c) Trees in parks, gardens and around buildings.

d) Tree plantations mainly for other purposes than wood, such as fruits orchards and palm plantations.

This study was focused on the first three categories as ToF are not assigned an area in the overall land use classification but occur inside other wooded land and other land. Although this definition is based on

trees, the concept likewise involves the site and other vegetation at the location. It is wise also to mention that, the definition of trees outside forest is dependent on the type of "forest" definition employed.

Trees outside forest may be predominantly natural and thus not maintained, such as woodlots, gallery forests and riparian buffers. Spatially, they may be dotted intermittently on farmland and pasture, or growing continuously in line-plantings along roads, canals and watercourses, around lakes, in towns, or in small aggregates with a spatial field such as clumps of trees, sacred woods, urban parks as in Figure 2; A, B & C (Alexandre *et al*, 1999).

1.4.3. High pass filter (hpf)

A fusion technique applicable to a wide range of sensor types including mixed sensors. It allows true colour against the sharpness of an image and ideal where there is a high discrepancy of pixel ration between the panchromatic (pan) and the multispectral (MSS) image.

1.4.4. Intensity hue saturation (ihs)

Just like hpf, it is applicable to a wide range of sensors but weighting is based on the overlap of the pan image wavelength with those of each of the MSS bands. The resulting colour retention is excellent although bands with little or no overlap with the pan image will receive less sharpening.

2. DESCRIPTION OF THE STUDY AREA

2.1. Geographic overview

Chitwan District is located between latitude 27°40'07.79" and 27°46'37.15" north and longitude 84°33'25.88" and 84°41'48.85" East (Subedi *et al.*, 2010) and is found some 150 Km from the West of Kathmandu, the political capital of the Country. The District shares a common boundary with Dhading, Gorkha and Tanahun Districts in the north, Makwanpur to the East, Nawalparasi to the West and the international border of India to the South. It is one of the richest districts of the country with extensive natural and commercial forests and diverse agricultural productivities (ICIMOD et al., 2010).

The Kayarkhola watershed covers an area of 2,381.96 hectares and is located in the Chitwan District of Nepal in the Central lowland of Nepal. Amongst the five major ecological zones found in Nepal, the Kayarkhola watershed is characterised by both the tropical and sub-tropical with abrupt altitudinal variation (Subedi, *et al.*, 2010). The Kayarkhola watershed is divided into 15 Community Forest User Groups (CFUGs). The CFUGs promote the suitable utilisation and equitable distribution of resources available from the community forests to improve the socio-economic situations of deprived sections of the community. The activities of the CFUGs are controlled by the Federation of Community Forestry Users, Nepal (FECOFUN) and Asian Network of Sustainable Agriculture and Bio-resources (ANSAB).
The annual average temperature is 24°C with a range between 16°C and 32°C. Precipitation also varies from 1584 to 2287mm with an annual average of 1830mm. Moreover, the altitude of the watershed as a whole ranges from 245m to 1944m with an area of 8002 hectares. The climate of the district is monsoon with evergreen and semi-deciduous tropical forests (IPCC, 2006).

2.2. Land use

Forest is said to constitute about 60% (128,500 ha) of the District of Chitwan (ICIMOD, et al., 2010). The forest is made up of the Chitwan National Park that is known to be a world heritage with an area of 970 Km^2, part of the Parsa Wildlife Reserve and the various community forests. However, the Kayarkhola watershed accounts for 66.9% (5,195) ha of forests, 0.0005% (3.8) ha of barren land, 3.4% (264.4) ha of bushland, 29.2% (2,268.6) ha of farmland for cultivation and 0.43% (33.3) ha of grassland. During the growing period, the farmers prune the tree crowns for fuel wood, fodder or just to allow the penetration of sunlight into their fields.

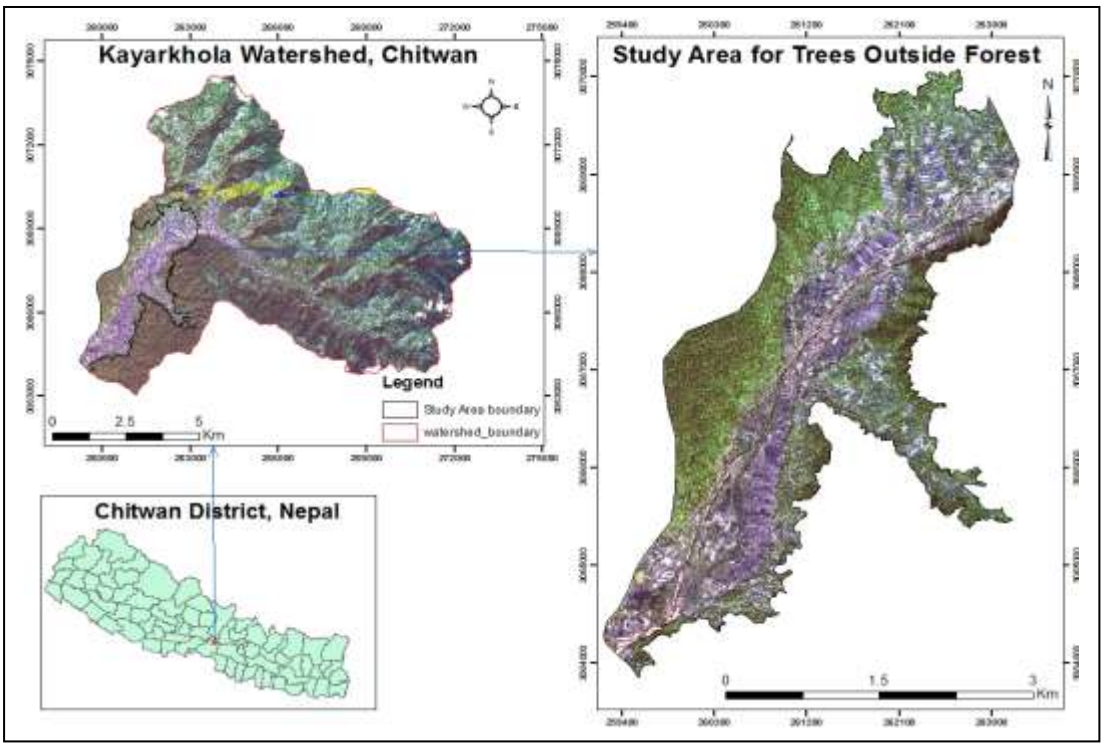

Figure 1: Location of the study area in Kayarkhola watershed, Chitwan District, Nepal

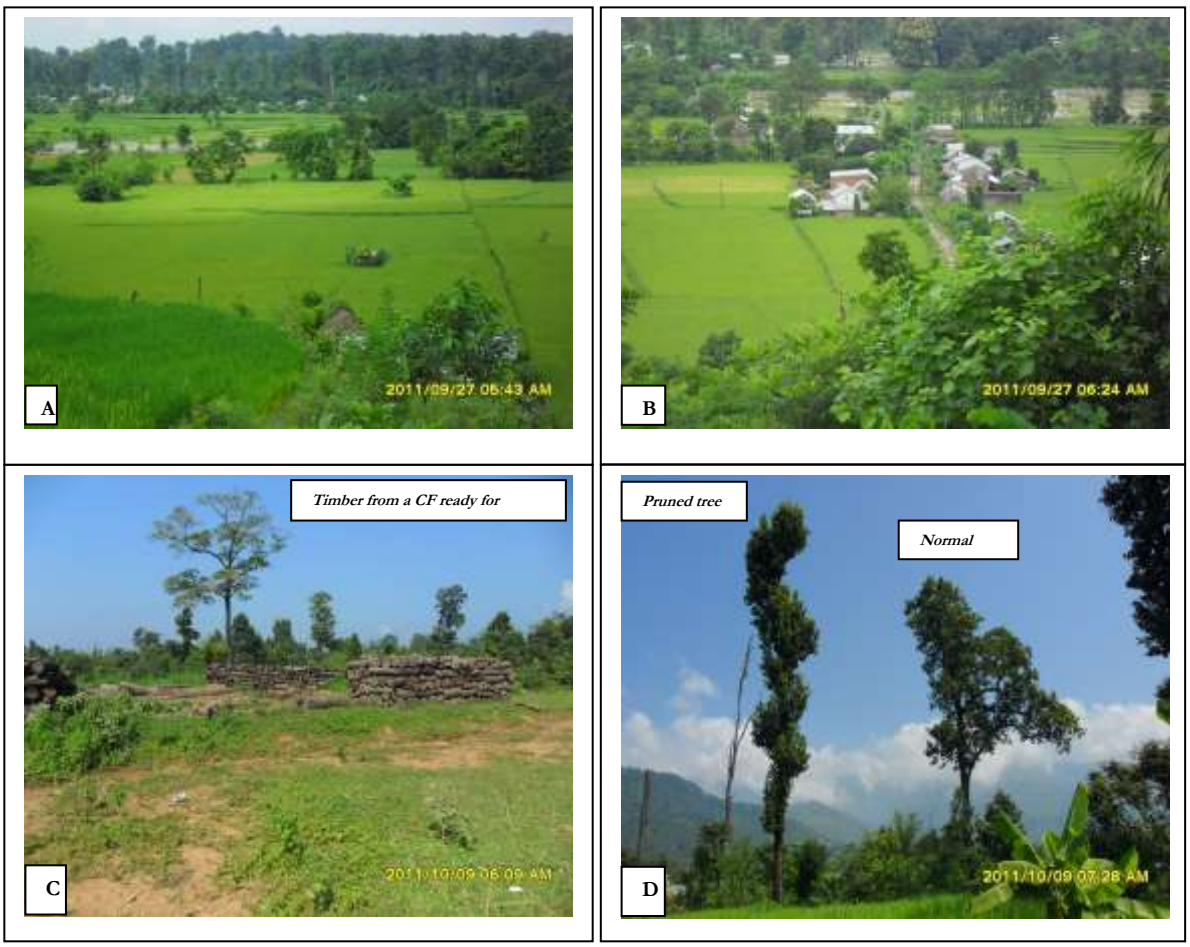

Figure 2: Photos of the study area

2.3. Socio-economic:

The actual population of the study area is estimated to be about 22,090 inhabitants with actually 3,935 households, though there is some uncertainty in this estimate (ICIMOD, et al., 2010). Moreover, the population is mostly made up of the forest-dependent indigenous communities. They are basically farmers who practice their traditional shifting cultivation as they continue to extend from the lowland into the hills with their rice fields. Within the study area, the dominant ethnic groups are the Chepang that is considered a vulnerable group and the Tamang (Subedi, *et al.*, 2010).

2.4. Vegetation

The vegetation of the watershed range from hardwood forest in the lowland through coniferous and mixed broad leaves forests in the mid to upper elevation (ANSAB, 2010). *Shorea robusta* is a dominant tropical hardwood species in the area. There are also some dominant associates like *Lagerestroemia parviflora, Mallatus phillipinensi* and *Terminelia tomentosa* in Kayarkhola. However, there has been some introduced tree species (e.g. *Dalbergia sissoo* and *Techtona grandis*) that were principally encountered in the rice fields and are used as fuel wood and fodder for the livestock (Appendix 1).

3. METHODS

3.1. A Flowchat of activities

The flowchart of activities is presented on Figure 3. It consists of the independent processing of the remotely sensed data (airborne LiDAR and Geo-Eye) and the procedures involved in calculating carbon stock from the field measured data. These processes are then related through a regression analysis for the estimation of carbon stock.

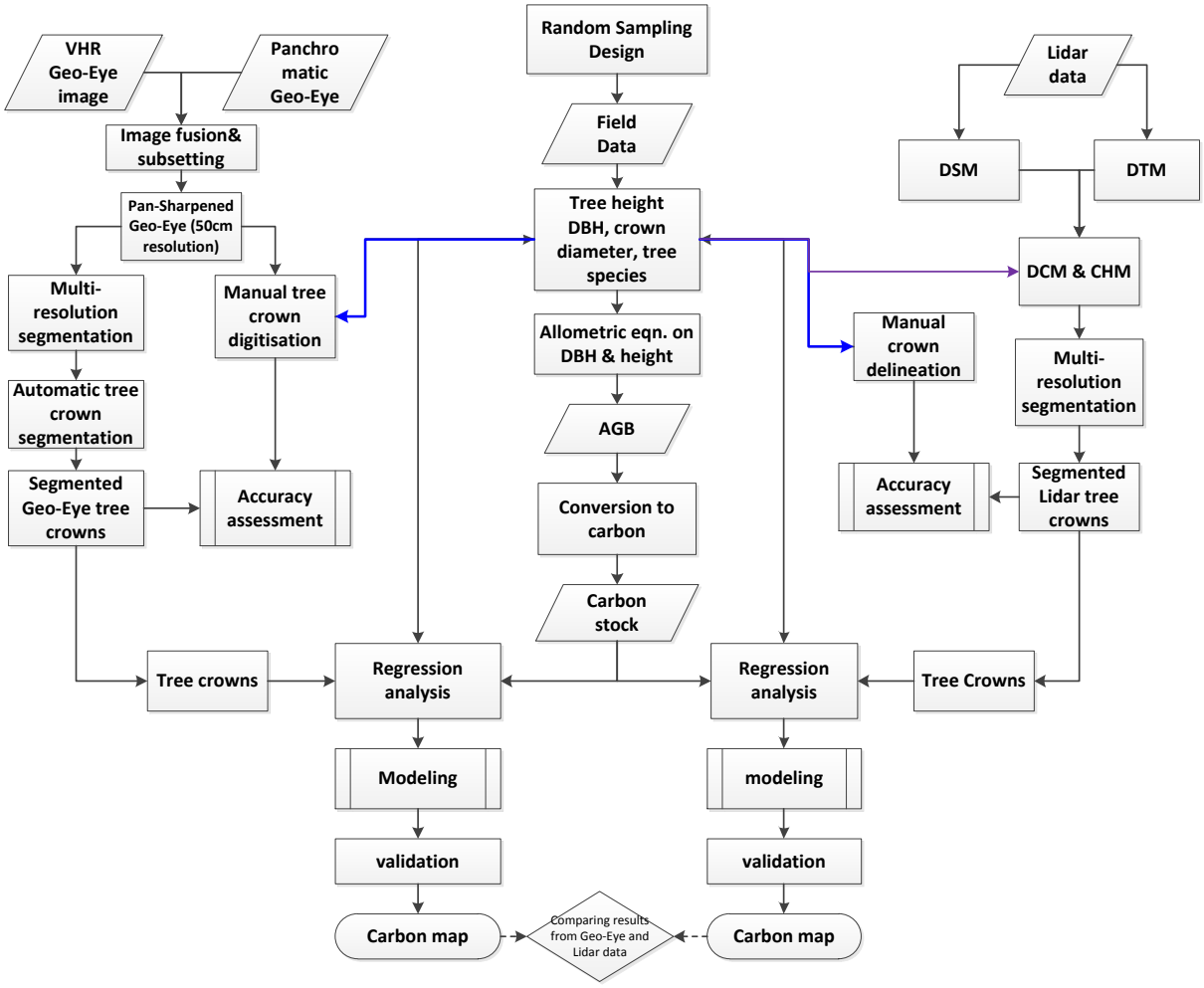

Figure 3: Flowchart of activities

3.2. Sampling Design

Spatial boundary of the study area were on-screen delineated to ease measuring and verification (Subedi, *et al.*, 2010). Basic topographic information was superimposed on the image to facilitate navigation in the

field. An iPAQ was used for navigation and to locate the clearly identified stand-alone trees. Coordinates of some trees were recorded on the iPAQ. The pan-sharpened image from VHR Geo-Eye was transformed into the Enhanced compression wavelength (ECW) for it to be easily loaded into the iPAQ. A random sampling technique (Kohl et al, 2006) was used to obtain the tree parameters for the inventory in the study so that every tree in the sample can have an equal chance to be measured. Tree samples were measured based on their availability and their natural structure (i.e. not pruned) within the vicinity (Figure 2; D). Efforts were made to cover all the study area during data collection for a concise, concrete and statistically acceptable analysis. This was based on maximum variation on our area of interest at different patterns of homogeneity and possibility. Trees with DBH of less than 10cm, height of less than 5m and pruned tree crown structure were not considered in the sample size.

3.3. Pre-field work

The satellite images were used to demarcate our study area using on-screen digitisation. Some single trees and a group of trees were identified in-order to cover the whole study area and then printed for easy recognition of the trees in the field.

The ECW format of the pan-sharpened image was uploaded into the iPAQ to enable identification of the trees. Printed maps in JPEG format of the digitised polygons of less than 0.5 hectares were also used for trees identification. Some easily identified trees and their coordinates were recorded on both the iPAQ and the data sheets.

3.4. Field data collection

The printed maps from the VHR satellite images alongside with the iPAQ and Garmin 12*XL* GPS were used as a guide to locate the various digitised points and polygons. Subedi *et al.*, (2010) confirmed the use of GPS tracking as an efficient and accurate method for boundary location. Unfortunately, most of the delineated tree polygons on the satellite images before field work were discovered to be bamboo forest patches during the field practice. Much emphasis was then laid on the un-pruned stand alone trees that were equally part of the original sample size and found to be randomly distributed in the study area. The sample size was a function of the tree density, shape and availability (MacDicken, 1997), as the study area is a sparse vegetation in rice fields.

Trees with a DBH of 10 cm and above were measured and recorded while the other parameters of tree height and crown diameter were recorded on the field. In addition, the well-recognised trees on the iPAQ of each identified sample from the Geo-Eye satellite image were recorded (Mora, *et al.*, 2010; Popescu, 2007). Care was taken to ensure that the diameter tape was placed around the stem at exactly on the indicated point of measurement at 1.3m above the ground level. The tree heights were measured from the tree base to the tip of the highest point using the Haga altimeter. Tree crown diameter was computed from a half of the measurements of the crown projection area (CPA) in the direction of North-South and West-East or a sum of the measurement of the radii of the CPAs in all four cardinal directions and then divides by 2.

3.4.1. Field data analysis

The data collected was entered into an excel spread sheet and descriptive statistics was employed for a data summary and to check the bias function of the estimator. Excel, SPSS and R software statistical packages were also exploited for the strength of the regression analysis between the field measured parameters and further relate to the remotely sensed data.

3.5. Data processing

3.5.1. Data pre-processing

The airborne LiDAR data had about 53 million LiDAR measurements for the study area, and the number of grid cells to hold each data per measurement is 3.5 million. The brightness of the data was visualised for its quality in 3-D from which some stripes were realised on the data (Figure 4: A). The data was splited into tiles with user-specified size on which filtering through clipping was then applied. "It is impractical to apply progressive morphological filtering to process all measurements as a single file because millions of points were collected for each survey" (Zhang et al., 2003). Data of the upper most layers of the point clouds (Figure 4; C) were removed as repeated measurement for each cell because the dataset included multiple returns of the same laser pulse. (1999) reported that among the several thousand returns obtained from a high tree canopy forest like in the tropics, a maximum of just one return is from the ground. This implies during the time of data capture, some particles other than the first and last return were recorded as vegetation height. A final digital terrain model (DTM) was estimated at 1,293.8m *asl.* The bare-earth points were classified more accurately as they were considered from the ground surface.

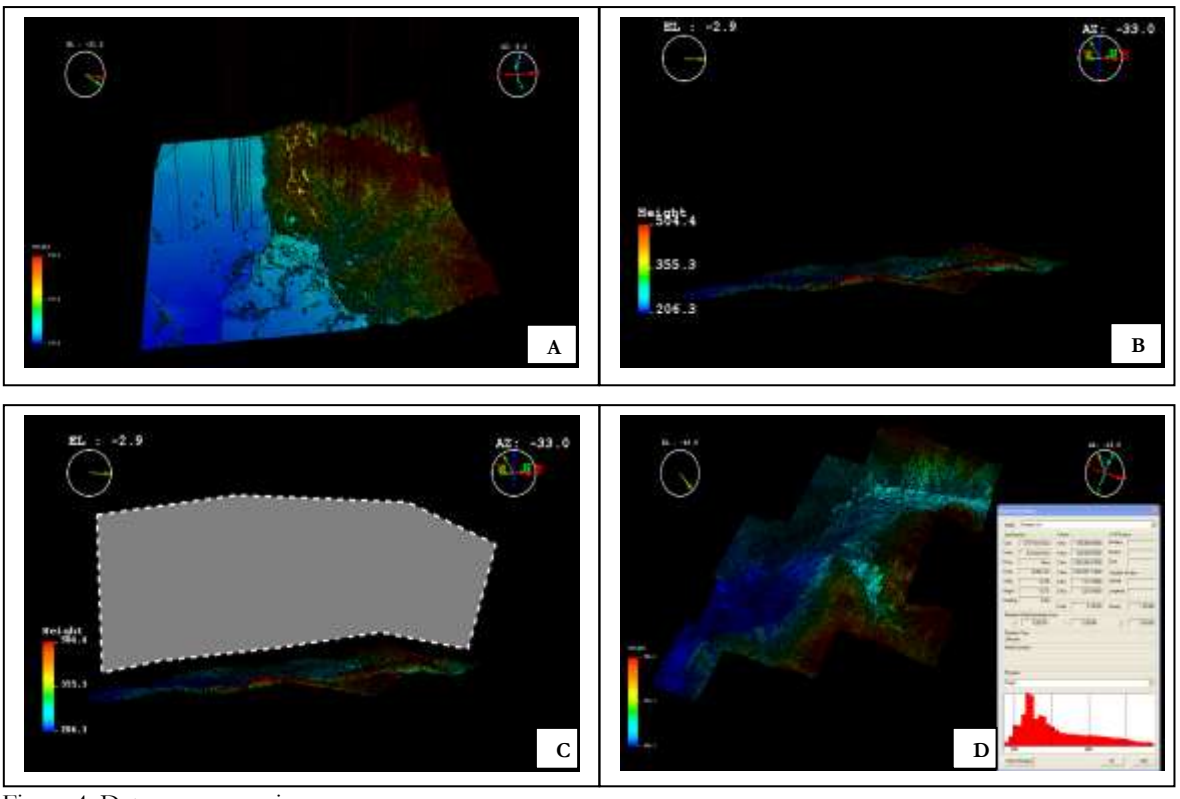

Figure 4: Data pre-processing

(A) *LiDAR stripes in the data* (B). *Surface points* (C). *clipping-out process* (D) *Cleaned image of 2-D & elevation representation*

Pre-processing was not done on the VHR satellite Geo-eye image as the obtained images were already radiometrically corrected.

3.5.2. Processing of Canopy Height Model from airborne LiDAR data

In the process of interpolation of the raw airborne LiDAR data after filtering, the first and the last return LiDAR canopy height data were respectively re-sampled into regular grids as digital terrain model (DTM) and digital surface model (DSM) (Chen et al., 2003). A TIN-based interpolation was applied to rasterise the airborne LiDAR data at a 50cm resolution. The ground control points were then used to construct a mathematical model for space registration thereby building up a relationship between airborne LiDAR space and image space. The DSM was extracted from the first pulse reflections while the DTM was processed using the last returns. The difference in height between DTM and represent the absolute height of the tree described as the normalised digital surface model (nDSM) (Chen *et al.*, 2003).

3.5.3. Image fusion Geo-Eye

Pan-sharpening or image fusion combines the geometric details of a high resolution panchromatic (pan) image and the colour information of a low resolution multispectral (MSS) image to generate a high resolution MSS image (Neteler & Mitasova, 2008). Image fusion is aimed at increasing the likelihood to apply the remotely sensed images as most information acquired from individual sensor applications are incomplete, inconsistent or imprecise (Pohl & Van Genderen, 1998). The high spectral and high spatial information of the MSS images was preserved to be used in GIS applications for easy interpretation. The stacked MSS (2m resolution) image was then fused with the Geo-Eye pan image of 0.5m spatial resolution to obtain a spatial pan-sharpened MSS image of 0.5m spatial resolution. The fusion methods of intensity hue saturation (IHS) and high pass filter (HPF) in ERDAS IMAGINE 2011 were used and their results applied independently on different subsequent processes depending on visualisation of forest characteristics and settlements.

3.5.4. CPA delineation

3.5.4.1. Image filtering

This technique performs enhancement operations such as averaging, high-pass (edge enhancing), low-pass (smoothing) filtering to upgrade the visual interpretation of an image by increasing the distinction between features and removing noise. Through averaging or a smoothening process, a 3*3 low-pass spatial filter was used in ERDAS IMAGINE 2011 to remove small random spatial variations of noise and some high frequency signals in the convolution process (Neteler & Mitasova, 2008). For homogeneity of the image segments with the VHR images, a median filter was applied to reduce the amount of convolutions in the final segmented polygon (Mora, *et al.*, 2010). Thus a median filter of 3-by-3 was used for the tree crown delineation in ERDAS for this study as a control to the unfiltered image.

3.5.4.2. CPA delineation

The pan-sharpened filtered and unfiltered images were displayed in ArcGIS10 and viewed at various scales for the shapes of the tree crown canopies. A scale of 1:250 was used all through the delineation process for a better visualisation. On-screen individual tree canopy digitisation was then carried out based on the visualisation potential on the unfiltered image with the assistance of the filtered image of the Geo-Eye where the texture of the object is properly seen on ArcGIS10. A total of 150 tree crowns segments were randomly delineated. Similarly, the truncated airborne LiDAR image was randomly on-screened digitised with a total of 145 segments. The airborne LiDAR image had no control as the tree crowns were properly differentiated and seen as whitish crown structures (Figure 5).

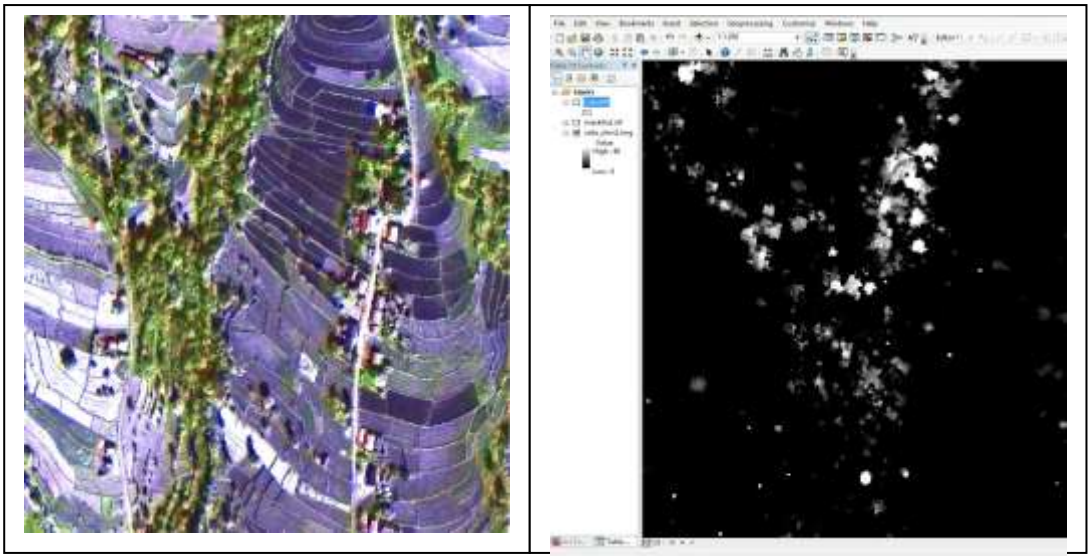

Figure 5: Representation of Geo-Eye (*left*) & airborne LiDAR image (*right*) before segmentation

3.6. Image Segmentation

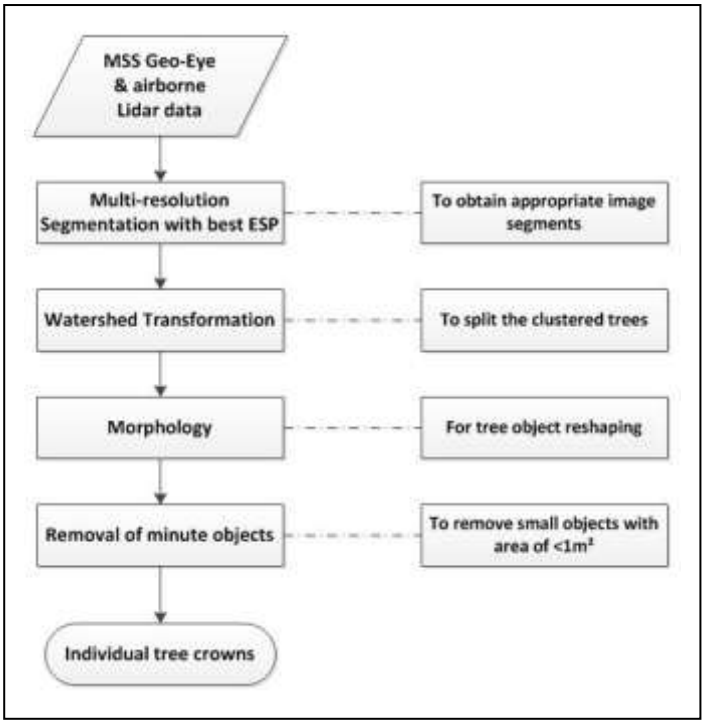

Figure 6: Overview of the segmentation process

The segmentation quality is based on the scale and heterogeneity of the image objects, the spatial and spectral aspect of the image, and the type of algorithms (Moller *et al.*, 2007). The process delineates units with homogeneous forest characteristic that is similar to forest stand delineated by on-screen manual digitisation (Wulder *et al.*, 2008b). This was done using the eCognition Definiens8.64 software in a multi-resolution segmentation method. Multi-resolution segmentation is based on geometry of the objects that overcomes the problem of over- and under-segmentation. Multi-resolution segmentation allows

classification of objects at different scales thereby generalising the levels (Zhang et al., 2003). Through a customised trial-and-error experimentation (Hay *et al.*, 2003), the parameters for scale, colour and shape were chosen in a multi-resolution segmentation process since the objects have to be meaningful. Figure 7 present the result of the rate of change and the local variance of the ESP (Kim, *et al.*, 2009), scale parameter of 18, shape of 0.5 and compactness of 0.9 was used for the VHR Geo-Eye satellite image for better identification of the object segments described to be the normal crown structures.

Likewise, a scale parameter of 10, shape of 0.1 and compactness of 0.5 was used for the truncated airborne LiDAR data. Region based multi-resolution segmentation was applied for the airborne LiDAR data as it uses region growing techniques to merge pixels with similar attributes (Lohmann, 2002) and is noise tolerant. A segmentation combination of elevation and radiometric attributes respectively from the airborne LiDAR data and the orthophoto-images were executed. Hence, pixels with similar height and spectral attribute were merged into a region resulting to object-based classification of each separated region. A knowledge-based classification based on elevation, spectral, texture and shape information was incorporated into the system to detect the separated regions.

3.6.1. The segmentation process

The segmentation processes are scale parameter setting, multi-resolution segmentation, watershed transformation and morphology. The independent step by step activity is illustrated below.

3.6.1.1. Estimator Scale Parameter (ESP) setting

This was done through experimentation to develop a protocol for segmentation using the ESP tools. These scales are the peak values obtained from the rate of change and the minimum local variance of the ESP tools (Figure 7). Compared to the Geo-Eye, the rate of change of the airborne LiDAR was steeper resulting to larger tree crowns with slight change in the scale parameter. However, in both the airborne LiDAR and Geo-Eye data types, the scale parameter developed from the subsets of the images did not apply for the whole study area maybe due to poor representation. Hence, new scale parameters were developed for the whole study area as indicated above.

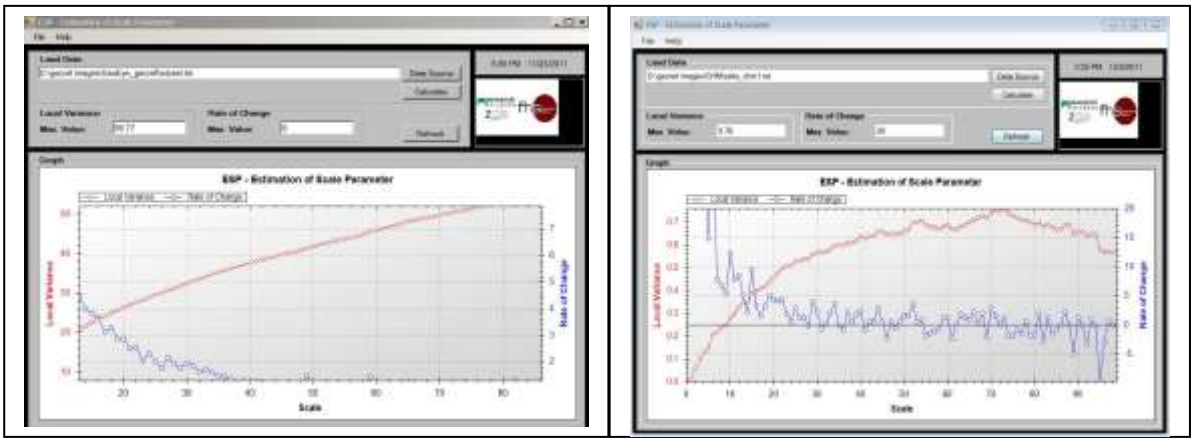

Figure 7: ESP tools for Geo-Eye (*left*) and LiDAR data (*right*)

3.6.1.2. Multi-resolution segmentation

During the process within the object features, the customised algorithm was computed to normalised difference vegetation index ("NDVI") as it is one of the simplest and fastest means for vegetation identification. NDVI is the most commonly used index to distinguish existing canopies of green plant in MSS remote sensing data. Layer values for "Brightness" were used to describe the object segments for the Geo-Eye. The image layers were similarly weighted at 1.

For the airborne LiDAR data, "Brightness" and "maximum pixel values" from the object features were used to distinguish the image objects. Maximum pixel value gives us the maximum height of each tree with it distinct brightness. Areas out of the truncation threshold (6m and >40m) were seen as dark on the LiDAR image. Since our minimum tree height from field was 6m, values below 6m were eliminated as either grass or another shrub that was not considered as a tree in the process.

3.6.1.3. Watershed transformation

This process considers the gradient magnitude of an image as a topographic surface. Pixels that are draining to a common local intensity minimum form a catchment basin that embodies a segment. The process is aimed at re-shaping the tree crowns. The intermingled tree crowns are separated into individual tree crowns using a splitting threshold. The threshold is dependent on the expert knowledge of the crown diameter. In this process, a length factor of 16 pixels was used as the average crown diameter from the field data was roughly 8 metres.

3.6.1.4. Morphology

The process smoothen the images into meaningful tree crowns. Closed image objects operation was applied for the study in order to fill the smaller holes created by the shadow and difference in spectral properties. A circular masking of 16 pixels was used for standardisation of the tree crowns since circular shapes best describe tree crowns. Objects with crown diameter of less than $1m^2$ (4 pixels) within another objects were merged into the same objects as one crown. This is because it apparently difficult to demarcate these objects on the image as another tree crown due to poor reflectance.

3.7. Accuracy Assessment

The accuracy of the automatic segmentation was tested with the use of reference polygons to the manually digitised polygons. Object differences were based on topological features of geometry on the degree of containment and overlap relationships (Figure 8).

Scores were recorded depending on the degree of coverage of the reference polygons; "if the complete reference polygon is covered by automatically achieved segments, best scores are given and vice versa" as in Figure 8 (Benz, *et al.*, 2004). When a digitised polygon occupies a 50% or more of the automatically segmented polygon, then it is considered as matching and otherwise the reverse. The manually digitised (150 polygons for Geo-Eye and 145 for airborne LiDAR) and the segmented shape files from Definiens of the respective data types were overlaid on a one-to-one matching of the polygons that represent the tree crowns to test the accuracy.

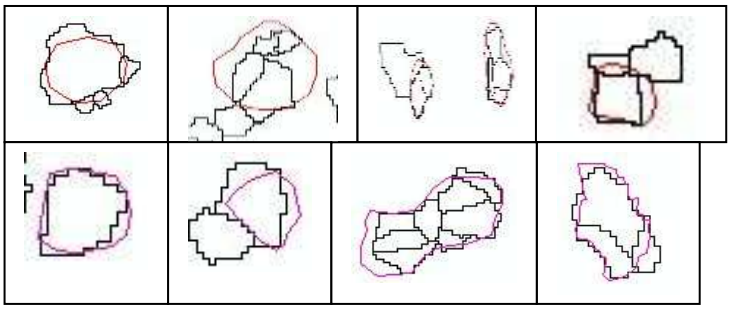

Figure 8: Topological relationship between two object levels

The automatically segmented polygons and the manually digitised reference segments were introduced into the Java Topology Suite (JTS) and GeoTools to validate the segmentation accuracy. GeoTools uses JTS Project to provide to an implementation of the geometry of the data structure. GeoTools is about implementing spatial solutions where nothing new is done than respecting the rules (JTS, 2012). Using Clinton *et al.*, (2005), the geometric segmentation accuracy assessment was defined based on the degree of over-segmentation, under-segmentation and a measure of the "goodness of fit" (D-value). The D-value is dependent on the proportion of over or under segmentation (eqn 1 & eqn 2).

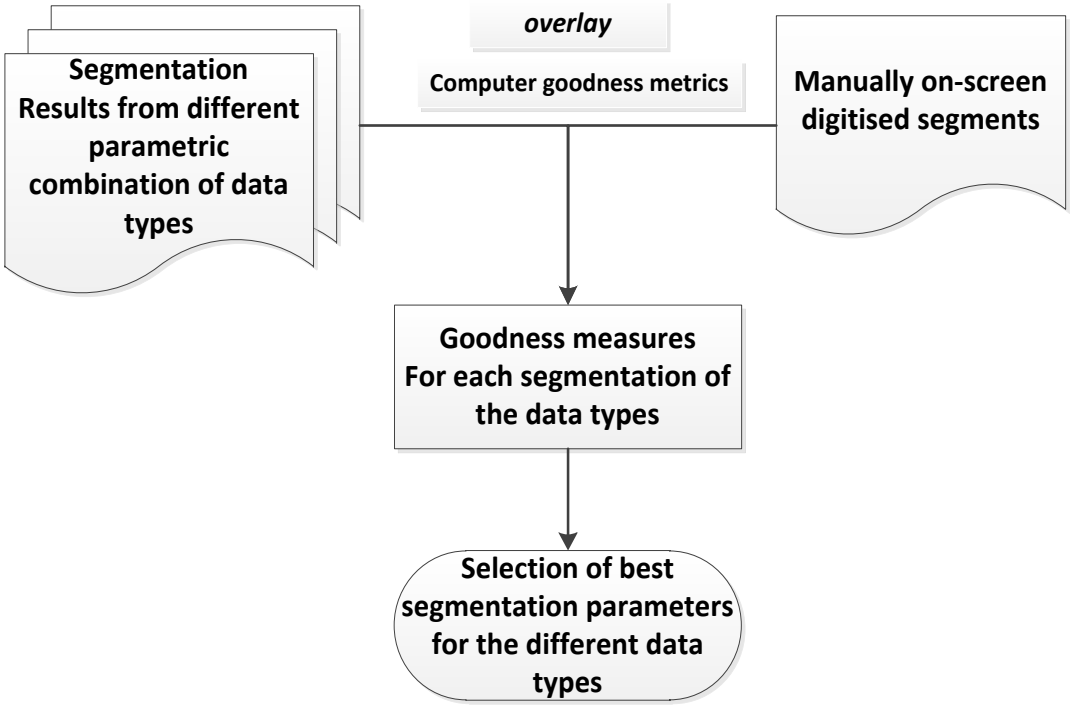

Figure 9: Method for accuracy assessment using JTS

$$\textbf{Over-segmentation} = 1 - \frac{area(xi \cap yj)}{area(xi)} \qquad \textbf{eqn (1)}$$

$$\textbf{Under-segmentation} = 1 - \frac{area(xi \cap yi)}{area(yi)} \qquad \textbf{eqn (2)}$$

Where:

x_i = digitised tree crowns (training objects) to judge the segmentation process
y_j = all segmented tree crowns from Definiens
$_I$ & $_j$ = 1 . . . . . n

Area ($x_i \cap y_j$) = area of geographic intersection of digitised x_i & segmented y_j object [see (Clinton et al., 2010) for the complete process].

The method of the root mean square (RMS) proposed by Weidner, (2008), was used to combine the over- and under-segmentation results defined as "goodness-of-fit".

$$\textbf{Goodness of fit (D)} = \sqrt{\frac{((oversegmentation^2) + (undersegmentation^2))}{2}} \qquad \textbf{eq}^{n}\ \textbf{(3)}$$

The index D is interpreted as the "closeness" of an ideal segmentation result in relation to the digitised tree crowns as training objects. D-index ranges between 0 and 1. Perfectly matching objects between the referenced and the segmented are accorded a value of zero. This implies under-segmentation and over-segmentation is non-existent. On the contrary, a D-value closer to 1 is given where there exists either an high over-segmentation or under-segmentation in relation to the largest intersecting segments (Clinton, et al., 2010).

3.8. Regression analysis

A regression mathematical model was performed between the field measured parameters (tree height, CPA and DBH) with field measured DBH as the dependent variable to determine the magnitude of the relationship. DBH alone constitutes about 50% of AGB in trees (Basuki, et al., 2009). A strong regression relationship between CPA and DBH means CPA can be used as a proxy for DBH in AGB and consequently carbon estimation. Likewise, field measured DBH was plotted against tree height and CPA from remotely sensed data. The validation of the relationship is based on the 30% data obtained from the field for verification.

3.8.1. Aboveground biomass and carbon stock calculation

The use of allometric regression models (equations) is a decisive phase in estimating AGB of a tropical forest, though its direct application is difficult (Brown *et al.* 1989; Houghton *et al.*, 2001). As such mixed species regression models were employed to compute tree biomass since there was the availability of the required data to be used in the various allometric equations and the diversity of the tree species (Subedi, *et al.*, 2010).

The base model used was from Chave *et al.*, (2005) and supported by Subedi *et al.*, (2010) for carbon estimation in Nepal. This is so because some authors suggested that including wood specific gravity into a model results to an increase in AGB estimation (Brown *et al.*, 1989; Chave *et al.*, 2005).

Thus, $\textbf{AGB} = 0.0509 * \varrho D^2 H$ ……eq^{n} **4**

Where: ϱ= wood specific gravity (Kgm^{-3})

D= diameter at breast height (DBH) (cm)

H= tree height (m)

AGB= aboveground biomass (Kg)

An area average wood specific density (ϱ) of 0.594 for upper slope mixed hardwood forest and ϱ=0.72 for lower slope mixed hardwood forest were available for the mixed tree species for Kayarkhola watershed. The equation above is more adequate as it makes use of the DBH and tree height of which a comparison of the tree heights will be made from that acquired from the LiDAR data.

There is a direct relationship with the quantity of carbon present in that biomass. Several studies on the estimation carbon on dry wood biomass have proven that carbon ranges between 45% and 50% for different ecosystems (IPCC, 2006; Westlake, 1963). The resulting AGB was then used to estimate carbon stock for trees outside forest using the conversion factor of 0.47 that was considered to be reasonable at regional scale by Kale et al., (2009) as represented in eq^{n} 5.

Carbon stock = 0.47 *AGB (MgC)……eq^{n} 5

3.9. Model validation

From the allometric equation of DBH and tree height, a relationship of the AGB and CPA resulting from the segmentation process was analysed using regression models/metrics. AGB was the response variable while CPA and tree height were the independent variable in a non-linear regression analysis for carbon estimation from any of the parameters that best describe the model.

The value of the segmented product is associated to data quality (e.g., noise, spatial and spectral resolution) as well as optimum customisation through trial-and-error of parameter settings, that permits variations of segmented results on target objects (Fortin *et al.*, 2000). However, delineated tree crowns with a one-to-one ratio spatial correspondence of segments were used to develop a model with 30% of the data for model validation. Validation was based on the resulting calculation from the field data with that obtained from the predicted carbon quantity by the model. The root mean square error (RMSE) of the carbon stock map was calculated and the closer the value of the RMSE is to zero, the more accurate is the model.

$$\mathbf{RMSE} = \sqrt{\frac{(Co - Cp)^2}{n}}$$

Where:

RMSE = Root Mean Square Error
Observed (Co) = indicates calculations based on field samples
Predicted (Cp) = indicates calculations from established models
n = number of observations in the sample

4. RESULTS

4.1. Image Segmentation

The two data sets (Geo-Eye and airborne LiDAR) were used for a multi-resolution segmentation processes independently with different scales depending on the ESP tool. The best scale parameters described above were employed to obtain the image objects (segments) that are the basic units for a segmentation process. Figures 10 & 11 shows some portions of the segmented tree crown objects derived from the process.

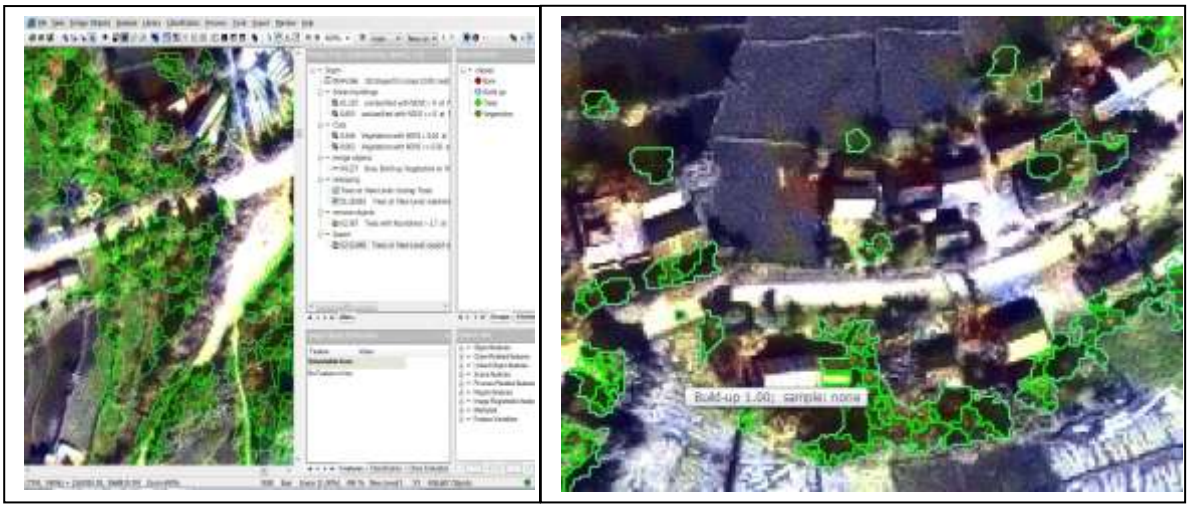

Figure 10: Segmented polygons of Geo-Eye (*green lines represent individual tree crowns or clusters*)

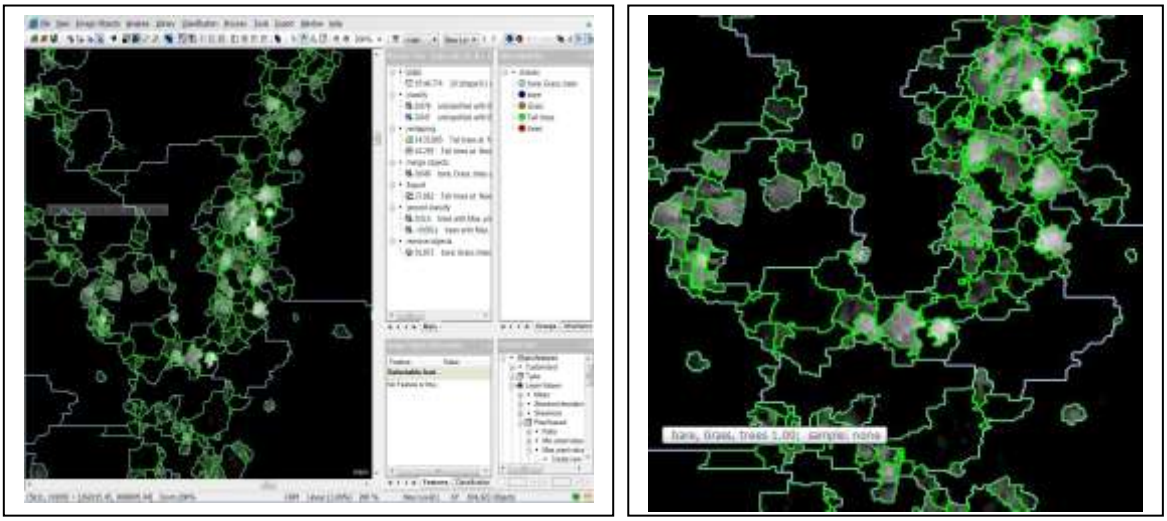

Figure 11: Segmented image objects from airborne Lidar (*green lines represent tree crowns & black colour for bare, build-up and vegetation*)

4.1.1. Segmentation accuracy assessment

As described in Möller *et al.*, (2007), the assessment of the segmentation accuracy was based on the tree crown geometry quality rather than the classification accuracy of the trees outside forest. Generally, the Geo-Eye had an accuracy of 73.9% from a total of 138 segmented tree crown objects clearly compared on a one-to-one matching of the digitised and the segmented tree crowns. Similarly, a 78.68% was obtained from the one-to-one matching of the segmented airborne Lidar data as reference tree crowns and the digitised tree crowns (Table 2). This implies the shaped 107 image objects of the manually digitised tree crowns coincided with the 136 segmented tree crowns from Definiens and 29 tree crowns were either over-segmented or under-segmented.

Table 2: Relationship of 1:1 on segmented and reference tree crowns

	Total reference CPA	Total 1:1 match	Correctly segmented CPAs
Geo-Eye	138	102	73.9%
LiDAR	136	107	78.68%

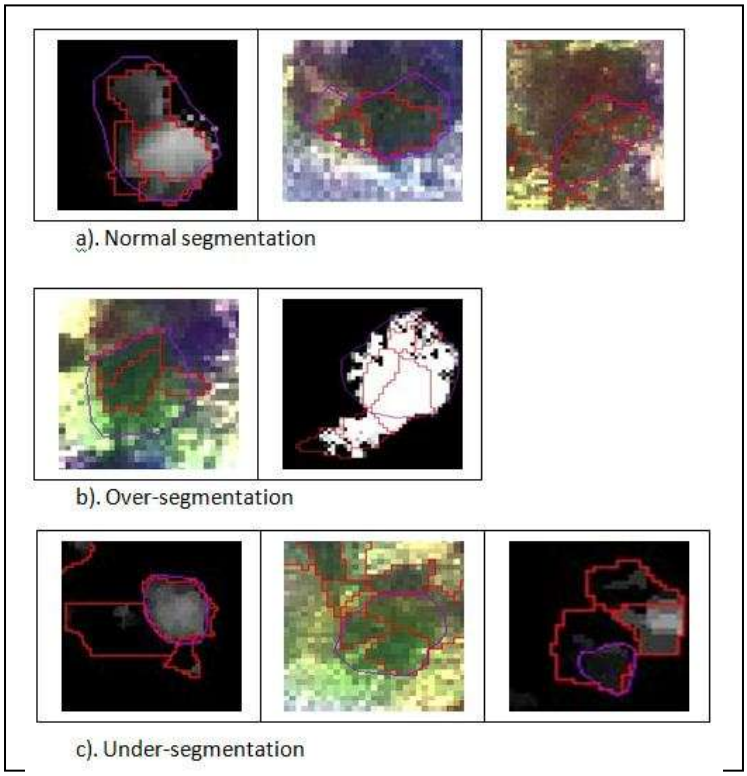

Figure 12: Visual interpretation of automatically segmented (*red lines*) and manually digitised objects (*purple lines*)

4.1.2. Segmentation validation

This was performed in the Java Environment with the use of the JTS and GeoTools (Figure 9). The stand-alone manually digitised tree crowns were used as reference tree crowns for the segmented product. The validation was effected with an over-segmentation of 0.4411 and under-segmentation of 0.1920 for the Geo-Eye while the airborne LiDAR data had 0.5028 and 0.1775 for over-segmentation and under-segmentation respectively (Appendices 5 & 6). Based on eq^{n} (3), a validation accuracy for the D-value on the tree crowns was 65.98% for the Geo-Eye and 62.29% was obtained from the LiDAR data (Table 3).

Table 3: Accuracy assessment from the Java environment

Data types	Over-segmentation	Under-segmentation	Goodness of fit (D)
Geo-Eye	0.4411	0.1920	0.3401(65.98%)
LiDar	0.5028	0.1775	0.3771(62.29%)

4.1.3. Abnormalities in Segmentation Process

For the airborne LiDAR data, all the field measured trees were recognised and automatically segmented in the segmentation process. But, it was realised that 13 trees (2.95%) out of the totally field measured stand-alone trees outside forest were not segmented for the VHR satellite Geo-Eye image. Twenty-six percent (36 trees) of the measured single trees were considered as a cluster of trees for the Geo-Eye while the airborne LiDAR data had 29 (21.32%) trees. Table 4 presents the individual proportionality of the tree cluster formed by Definiens software while Figure 13 shows some trees that were not captured during the segmentation process or that were considered as more than one tree.

Table 4: Segmentation abnormalities for trees outside forest

Data types	N° of trees not segmented	N° of single trees segmented as clusters
Geo-Eye	13 (2.95%)	36 (26.08%)
LiDAR	None	29 (21.32%)

Figure 13: Representation of segmentation abnormalities on Geo-Eye image

Furthermore, based on a comparison of the proportionality of the on-screen digitised and the automatically segmented CPAs, the ratios of 1:2, 1:3, 1:4 and 1:>4 were obtained. The ratio of 1:3 had the highest in Geo-Eye image with 11.59% while 1:2 ratios was recorded as the highest for airborne LiDAR data which had 11.03% (Table 5). However, ratios of 1:4 and greater were minimal signifying the accuracy level of the method. These ratios could have been a result of the many branches of the mostly dominated deciduous trees that were considered as individual CPA especially by the LiDAR beams during the image capturing process.

Table 5: Proportion of segmented to digitised tree crowns as clusters

Data types	Digitised CPA : Segmented CPA					
	1:1	1:2	1:3	1:4	1:>4	Total
Geo-Eye	102 (73.9%)	14 (10.14%)	16 (11.59%)	4 (2.89%)	2 (1.45%)	138
LiDAR	107(78.68%)	15 (11.03%)	5 (3.68%)	4 (2.94%)	5 (3.68%)	136

* *Percentages are based on the segmented total of 138 for Geo-Eye and 136 for LiDAR*

4.2. Extraction of CPA from datasets/ Comparing CPAs from field data & RS data

4.2.1. Model development and validation for CPA

From the segmented CPAs of both the airborne LiDAR data and the VHR Geo-Eye satellite image, the model relationship between the field CPA (from field diameter) and the results of the remotely sensed data were computed. A regression was run with 142 airborne LiDAR and 129 Geo-Eye samples that coincided during the different on-screen digitisation processes of both data sets were used for this analysis. The result of the linear regression gave an R^2 of 0.7434 and 0.7327 for the airborne LiDAR data and the Geo-Eye respectively (Figure 14). This shows that 74.34% of airborne LiDAR and 73.27% of Geo-Eye of the variations of the field measured CPA could be explained by the data sets. The RMSE was 38.24% and 41.18% for the LiDAR and Geo-Eye respectively. A descriptive statistics of the various data sources gave different means, standard deviation and standard error (Appendix 8). The linear regression statistics between the field measured CPA and remotely sensed CPAs ($p < 0.05$) are represented on Table 6 below.

Table 6: Linear regression statistics of field measured CPA and remotely sensed CPAs

Regression statistics		Coefficients		*t*-stats	p-value
Multiple R	0.8559	Intercept	19.796	6.16	9.06^{-9}
R Square	0.7327	CPA_Geo-Eye	1.13	18.66	3.4^{-38}
Adj. R Square	0.7306				
Standard Error	25.8265				
Observations	129				
Multiple R	0.8633	Intercept	7.223	1.979	0.0497
R Square	0.7453	CPA LiDAR	1.18	1.05^{-43}	1.05^{-43}
Adj. R Square	0.7433				
Standard Error	26.355				
Observations	143				

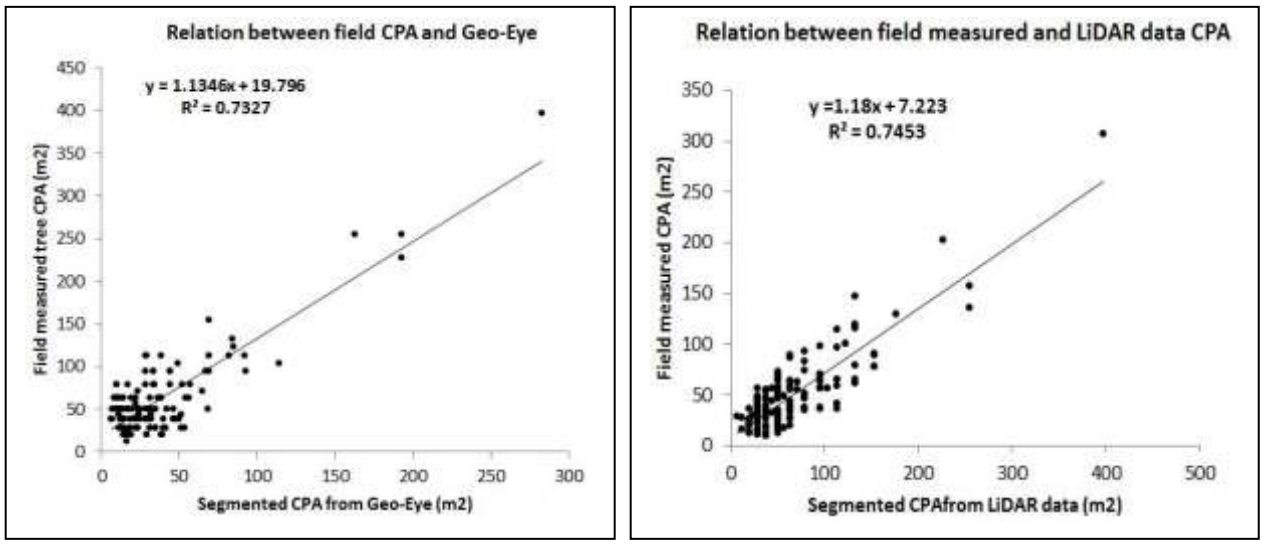

Figure 14: Segmentation relationships between field CPA & Geo-Eye (*left*) and field CPA & LiDAR (*right*)

The mathematical linear regression models developed goes thus:

Field CPA = 1.13 * CPA $_{\text{Geo-Eye}}$ + 19.8... ……..……eqⁿ 5

Field CPA = 1.18 * CPA $_{\text{LiDAR}}$ + 7.22 …….…….eqⁿ 6

4.3. Comparison of field measured and remotely sensed data

4.3.1. Extraction of Canopy height model (CHM) from LiDAR data

The height of the trees from the airborne LiDAR data was obtained using local maximum filtering since during our field survey, the tree height was obtained from the top of the tree. This value represents the highest point of a tree crown and the dark area represents vegetation canopy below and above the truncation threshold (Figure 15). A box plot of the field height and the airborne LiDAR height irrespective of the species revealed their means as 15.28m and 15.02m respectively with a standard deviation of 5.89m and 6.23m. The average mean estimator error derived from a subtraction of the mean field height (h_{field}) and mean LiDAR height (h_{lidar}) was 0.26m. Variability was higher in the field height compared to the airborne LiDAR height and ranges from about 12 to 19 meters. However, the maximum tree height of the system was gotten from the airborne LiDAR data at roughly 35m.

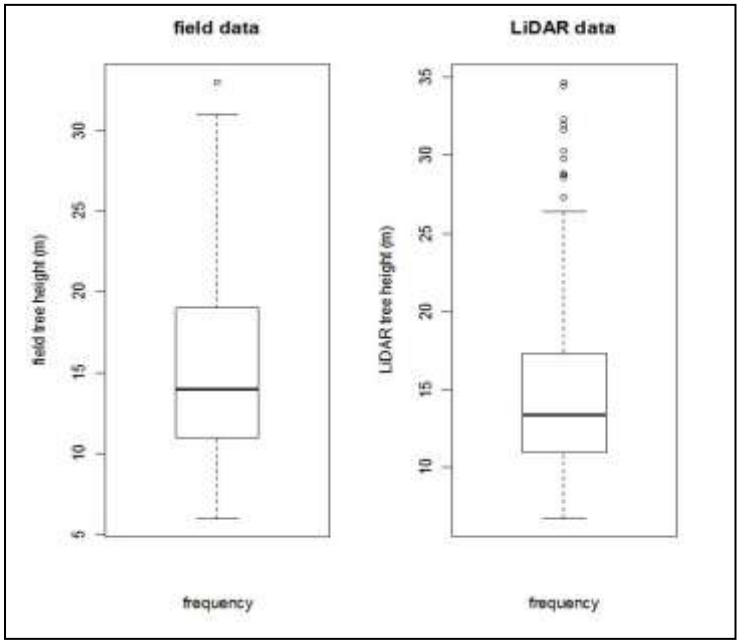

Figure 15: Box plots of mean field and LiDAR height

4.3.1.1. Model development and validation

To develop our mathematical model, 168 sampled tree heights obtained from the airborne LiDAR data were compared to that measured from the field. A strong linear relationship (R^2 = 0.912, P<0.0001) was observed between the field measured and the airborne LiDAR data estimated tree canopy heights in a scatter plot. This result indicates that roughly 91% of the variability in the sampled tree heights measured in the field was explained by using local maximum filtering of the CHM obtained from LiDAR data. A regression statistic was further performed for the significance of the result on field measured tree height and LiDAR height (Figure 16).

Table 7: Linear regression statistics of field measured and LiDAR tree height

Regression statistics		Coefficients		*t*-stats	p-value
Multiple R	0.9550	Intercept	1.716	4.85	2.81E-06
R Square	0.9121	LiDAR height	0.903	41.5038	1.45^{-89}
Adj. R Square	0.9116				
Standard Error	1.8543				
Observations	168				

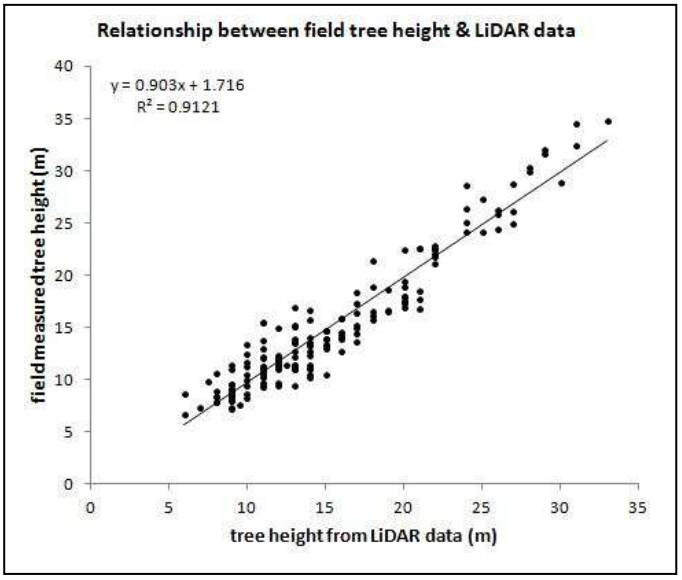

Figure 16: Scatter plot & regression table of field measured tree height & airborne Lidar data

So, the mathematical regression model developed for tree heights estimation for tree outside forest using airborne LiDAR data with a RMSE of 13.59% is given as in the equation (eqn 7) below.

Field height = 0.903* LiDAR $_{\text{tree height}}$ + 1.72 ……..eqn 7

4.3.2. Comparison of DBH with CPAs

4.3.2.1. Comparisons of DBH with field measured CPA

In order to test the accuracy for the relationship between the field data and the remotely sensed data, a mathematical regression model was fitted between DBH and CPAs from field measurements and delineated airborne LiDAR data respectively. The results of both data sets were significant in both the linear and non-linear regression models. However, the non-linear polynomial regression models gave a better result compared to the linear models and was further used for the model development. An R^2 of 0.533 and a RMSE of 35.65% was obtained for the field measurements of DBH and CPA from the non-linear polynomial regression (Figure 17; Table 8 below).

Table 8: Polynomial regression statistics of field measured DBH and CPAs of the 3 data sets

Relationships	R	R Square	Adjusted R Square	Std. Error of the Estimate	RMSE (%)	Sample size
Field measurement (DBH/CPA)	0.724	0.533	0.529	13.511	35.65	424
DBH/ CPA from LiDAR	0.731	0.546	0.5366	10.52	26.92	144
DBH/CPA from Geo-Eye	0.7235	0.521	0.5283	25.1789	46.91	124

The ANOVA table of the model between field measured DBH and CPA is found on Table 9 while curve fit is found on Figure 17 below.

Table 9: Result of ANOVA test between tree DBH & CPA of data sets

Parameter combination	Coefficients		t-stats	p-value
DBH/CPA from field measurement	Intercept	17.76	15.77	2.18E-44
	Field CPA	0.31	21.59	3.64E-70
DBH/CPA from LiDAR	Intercept	24.32	17.94	2.53E-38
	LiDAR CPA	0.26	12.40	2.14E-24
DBH/CPA from Geo-Eye	Intercept	24.63	15.898	1.62E-31
	Geo-Eye CPA	0.39	11.13	2.72E-20

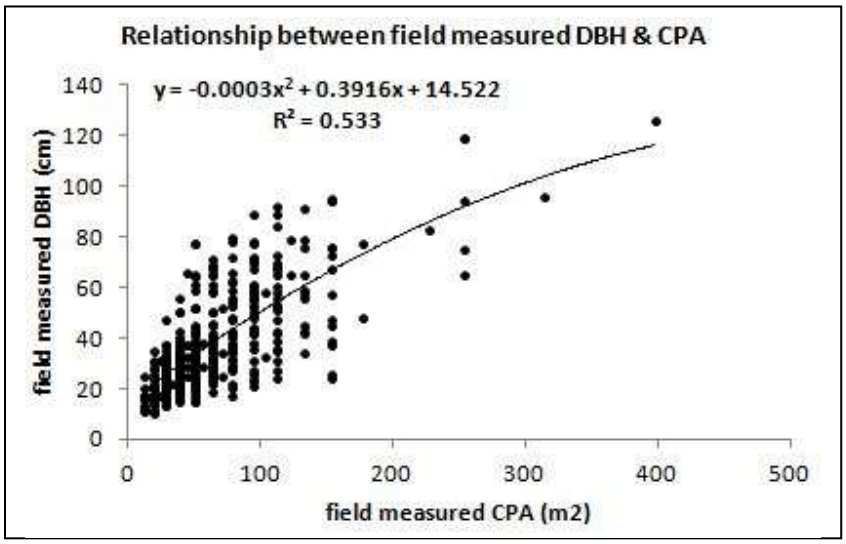

Figure 17: Non-linear regression graphs of field measured DBH/CPA

4.3.2.2. Comparisons of DBH with CPA from airborne LiDAR data

Non-linear regression model on the airborne LiDAR data produced an R^2=0.546 from field measured DBH and CPA with a RMSE of 26.94% using 144 samples (Figure 19; *right*). A regression statistic for the non-linear polynomial model is represented on Table 9 and the scatter plot on Figure 18; *right*.

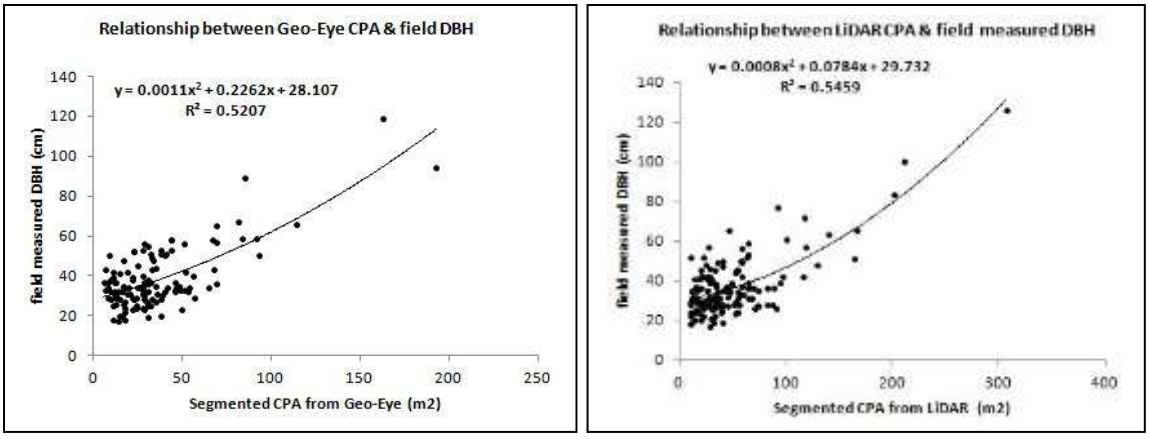

Figure 18: Non-linear regression graphs of field DBH vs CPA Geo-Eye (*left*) & LiDAR data (*right*)

4.3.2.3. Comparisons DBH with CPA from Geo-Eye data

Similarly, as in the airborne LiDAR data, the mathematical regression models carried out for both linear and non-linear produced a significant result. A non-linear polynomial model was proven to have the highest R^2 with values of R^2=0.521 for the relationship between field measured DBH and CPA from Geo-Eye (Figure 18; *left* & Table 9 above). The RMSE of 46.91% was obtained from a total of 124 samples.

4.4. Model development for biomass/ carbon stock

4.4.1. Application of allometric equations for biomass calculations

The total sample size was used to fit a mathematical model for regression analyses of the existing relationships between DBH, tree height and CPA with biomass and consequently carbon. The allometric equation developed in Chave *et al.*, (2005) for a tropical moist forest stand was used since there was the possibility to measure both the DBH and tree heights in the field for trees outside forest. The wood specific density (ϱ) of 0.72 for lower slope mixed hardwood forest was employed as our maximum altitude for the study site was less than 500m (ICIMOD, *et al.*, 2010). The mixed allometric equation was equally adopted by Subedi *et al.*, (2010) for carbon estimation for a tropical forest like Nepal though some authors recommended site specific allometric equation for a better accuracy (Basuki, *et al.*, 2009). In this respect, carbon stock per tree species was obtained from a multiplication of the biomass with a 0.47 factor developed by FAO (Kale, et al., 2009).

4.4.2. Relationship between carbon and CPA for Geo-Eye data

A regression analysis was fitted for a model to test the relationship based on the eq^n (4) above between the parameter biomass (carbon) and CPA for Geo-Eye data. The non-linear polynomial function was employed as it describes simple ecological situations where the response variable (carbon) depends on the combine effect tree structural parameters of the forest (DBH, tree height and CPA). The R^2 =0.5095 and $p<0.005$ was obtained for the non-linear polynomial (quadratic) equation and was significant at 95% confidence interval. This indicates that roughly 51% of the quantity of carbon from the field measurement is explained by the CPA of the segmented Geo-Eye image for trees outside forest. Table 10 gives a presentation of the quadratic regression analysis between carbon and CPA.

Table 10: Regression analysis of carbon and CPA for Geo-Eye data

	Unstandardised Coeff.		Standardised Coeff.		
	B	Std. Error	Beta	t-stats	Sig.
CPA.Geo-Eye	-18.368	30.735	-0.348	-0.598	0.554
CPA.Geo-Eye^2	0.521	0.427	0.711	1.221	0.230
(Constant)	579.307	476.847		1.215	0.232

The significance of R^2 of the result was tested using a one-way analysis of variance (ANOVA) at 95% confidence interval (Table 11).

Table 11: Result of ANOVA test of carbon and CPA for Geo-Eye data

	Sum of Squares	df	Mean Square	F	Sig.
Regression	4001166.189	2	2000583.095	3.154	0.055
Residual	2.283E7	36	634209.694		
Total	2.683E7	38			

Therefore, the model developed for AGB and consequently carbon stock (AGB*0.47) using CPA from Geo-Eye data is given below and represented as in Figure 19:

Carbon stock = 0.521* (CPA) ^{2} – 18.368*CPA + 579.307…….……eq^n 8

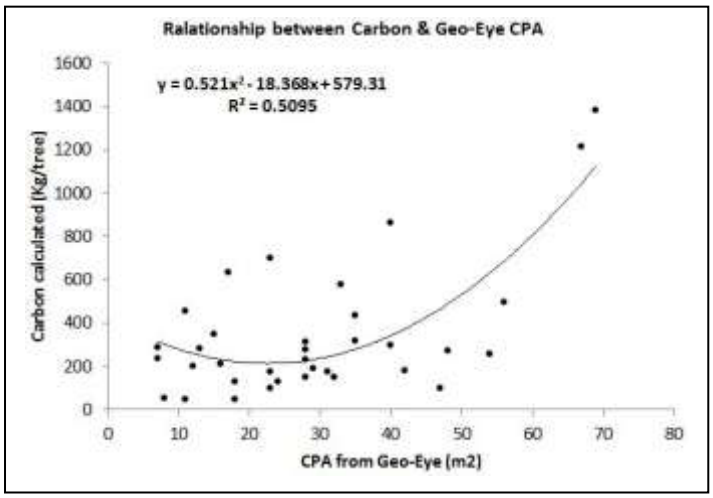

Figure 19: Graph showing relationships between carbon and CPA for Geo-Eye

4.4.3. Relationship between carbon with CPA and tree height for airborne LiDAR data

A regression analysis was carried out to model if there is a relationship between the parameters of carbon with CPA from airborne LiDAR data. We obtained an R^2 of 0.46 for the non-linear regression as best scores based on the 54 observations used as training data. Similarly, R^2 = 0.902 for the non-linear polynomial was obtained for a regression plot of carbon and tree height. The non-linear regression equation with the highest R^2 was accepted to be used for the model development since the quantity of carbon is explained by roughly 90% of tree height in the relationship (Figure 20).

Table 12: Polynomial regression analysis of carbon with tree height and CPA from LiDAR data

Tree parameter	Unstandardised Coeffs.		Standardised Coeffs.	t-stats	Sig.
	B	Std. Error	Beta		
Tree height	-285.988	58.870	-1.005	-4.858	0.000
Tree height^2	15.081	1.635	1.908	9.222	0.000
(Constant)	1504.468	475.854		3.162	0.003
CPA	-18.371	9.263	-0.516	-1.983	0.053
CPA^2	0.137	0.032	1.121	4.306	0.000
Constant	1238.515	389.438		3.180	0.003

Table 13 presents the result of a one-way ANOVA test. R^2 was very significant and almost zero at a confidence interval of 95%.

Table 13: Result of ANOVA test of carbon with tree height and CPA of LiDAR data

Tree parameter		Sum of Squares	df	Mean Square	F	Sig.
Carbon/Tree height	Regression	1.167E8	2	5.385E7	234.983	0.000
	Residual	1.266E7	51	248302.451		
	Total	1.294E8	53			
Carbon/CPA	Regression	5.951E7	2	2.976E7	21.727	0.000
	Residual	6.985E7	51	1369520.27		
	Total	1.294E8	53			

Thus, the model developed from the regression analysis for tree height and carbon stock based on the relationships of the airborne LiDAR data can be presented as in Figure 20:

Carbon stock $_{height}$ = 15.08*tree height^2 – 285.99*tree height + 1504.47……eq^n 9

Carbon stock $_{CPA}$ = 0.14*CPA^2 – 18.37*CPA + 1238.52 ……eq^n 10

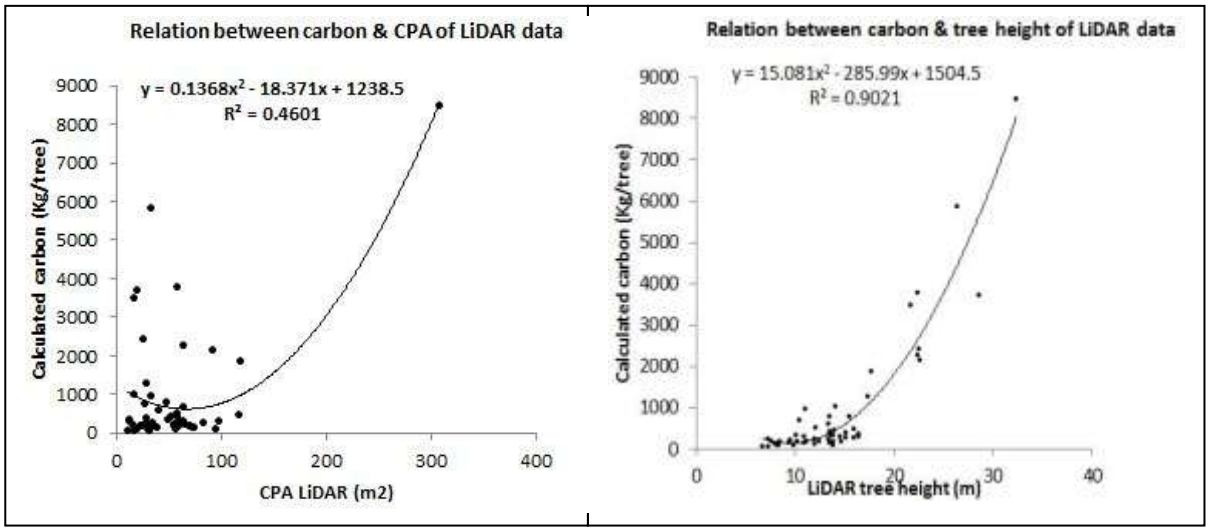

Figure 20: Graph showing relationships between carbon and CPA (*left*); & carbon & tree height for LiDAR data (*right*)

4.5. Model validation

4.5.1. Model validation for Geo-Eye data

Through a random selection by the R statistics package, 30% (25) of the data set was used to validate the model. A plot of the predicted values against the calculated carbon stock produced a model with R^2 of 0.97 (Figure 21; *left*). This is an indication that 97% of the calculated carbon from the field data is accounted for the predicted carbon based on a non-linear regression model. The "goodness-of-fit" between the predicted and the observed had a RMSE of 42.43%.

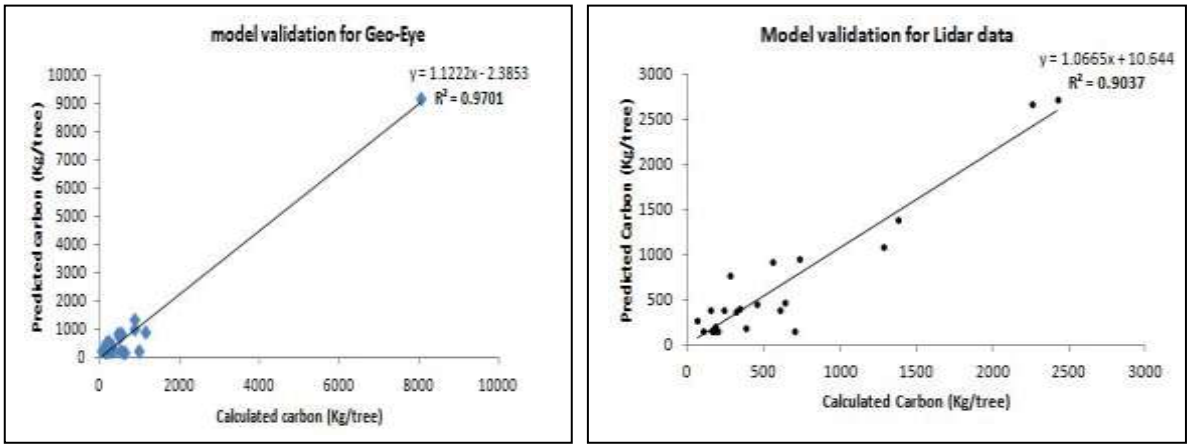

Figure 21: Scatter plot of model validation for Geo-Eye (*left*) and airborne LiDAR data (*right*)

4.5.2. Model validation for airborne LiDAR data

Similarly, a total of 24 samples were used from a random selection in R statistics to validate the model for airborne LiDAR data. An R^2 of 0.904 was obtained representing roughly 90% of the calculated carbon which is accounted for the predicted carbon using the model (Figure 21: *right*). The calculated RMSE of the model was 14.24%.

Moreover, a multiple regression was performed between carbon stock and the parameters of CPA and tree heights obtained from the airborne LiDAR data. The result gave us an R^2 of 0.689 with a RMSE of 11.53%. The model for the multiple regression models is thus represented in Table 14 and the scatter plot of CPA and tree height on Figure 22.

Table 14: Multiple regression statistics of tree height & CPA of LiDAR data

Regression Statistics	
Multiple R	0.830552
R Square	0.689817
Adj. R Squar	0.661619
Std. Error	368.5669
Observations	25

ANOVA

	df	*SS*	*MS*	*F*	*Significan F*
Regression	2	6646169	3323084	24.4629	2.55739E-06
Residual	22	2988514	135841.6		
Total	24	9634683			

	Coefficients	*Std. Error*	*t Stat*	*P-value*	*Lower 95%*
Intercept	-1048.28	282.8795	-3.70574	0.00123	1634.934284
CPA_LiDAR	0.7583	3.037651	0.249634	0.80519	5.541402699
LiDAR_height	117.2713	16.77965	6.988902	5.2E-07	82.47245531

Carbon stock = 117.27*Tree height $_{\text{LiDAR}}$ **+ 0.758*CPA** $_{\text{LiDAR}}$ **– 1048.28 ……eq^{n} 11**

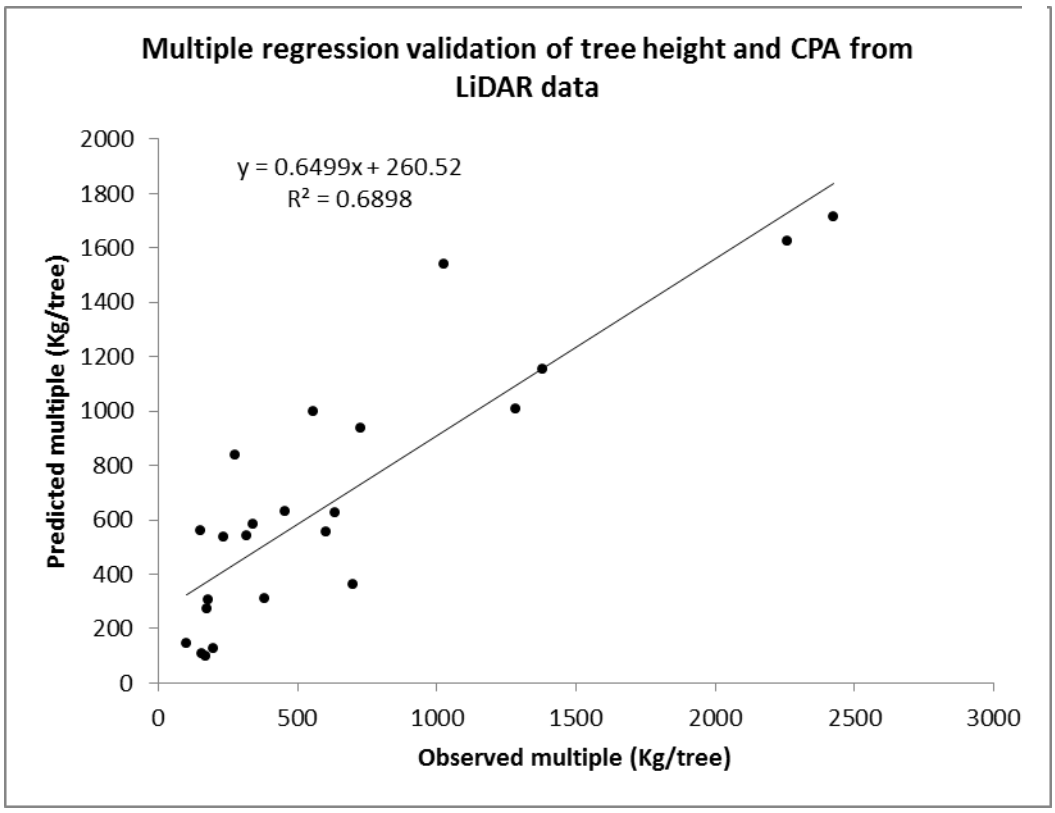

Figure 22: Scatter plot of multiple regression model validation from airborne LiDAR data

4.6. Carbon stock map

Carbon stock for trees outside forest was computed based on the 4 independent quadratic models (eq^{n}s 8 to 11). Three of the models came from the airborne LiDAR data based on the tree height and CPA parameters and the other from VHR Geo-Eye satellite image based on CPA alone. The highest quantity of carbon was obtained from the tree height estimation alone, followed by the multiple regression between

the tree height and the CPA from the airborne LiDAR data on a total surface area of 1007 ha. The quantity of carbon stored by the trees from the CPAs in both data sets was low. However, the best model was obtained when the multiple regression analysis was employed between the parameters (CPA & tree height) obtained from the airborne LiDAR data with a RMSE of 11.53%.

Table 15: Estimated quantity of carbon/ha from the various parameters

Data set	Parameter	Quantity of carbon (Kg)	Quantity of Carbon (tons/ha)	R^2	RMSE (%)
Geo-Eye	CPA	33,088,320	32.86	0.51	42.24
LiDAR	CPA	53,533,258	51.16	0.46	41.29
	Tree height	165,067,004	163.92	0.90	14.24
	Tree height & CPA	82,972,738	82.4	0.69	11.53

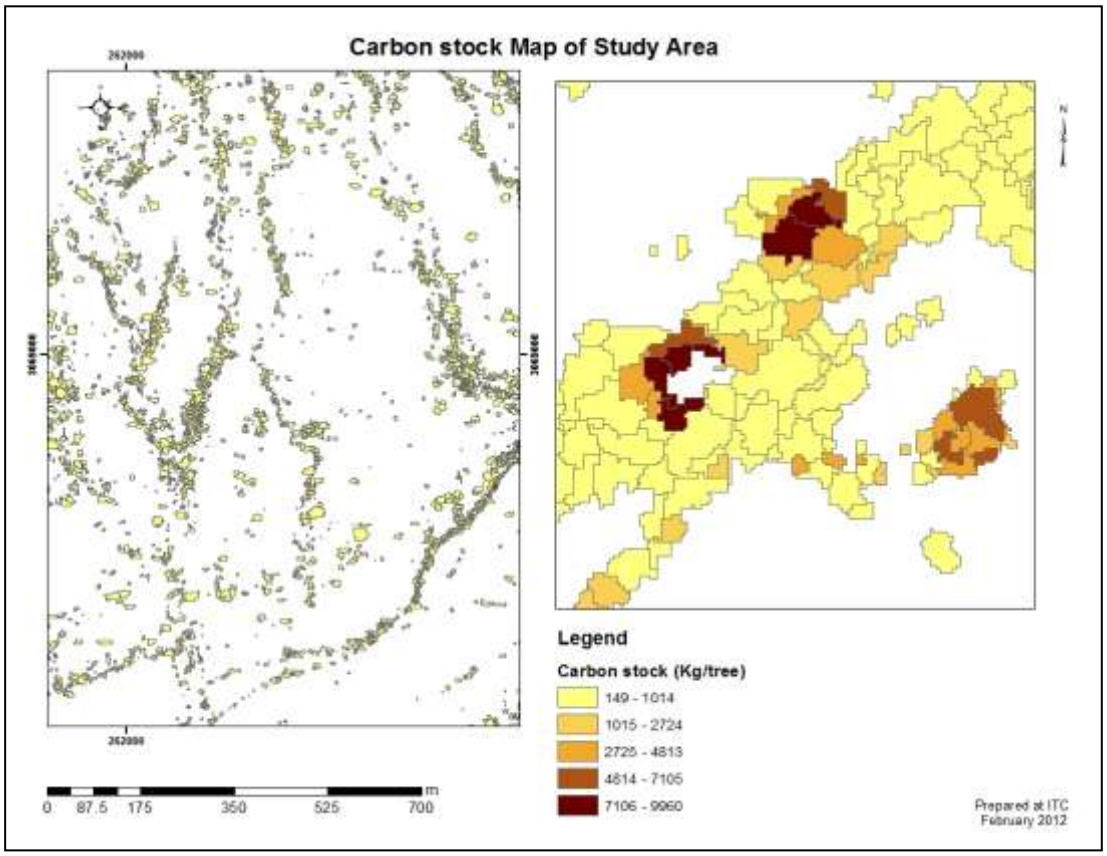

Figure 23: Carbon stock map of the study area

5. DISCUSSION

5.1. Rule set

Multi-resolution segmentation is highly dependent on the parameter combination that determines the maximum heterogeneity of the image. Though creating a rule set in segmentation has been very progressive and effective, the application is time consuming as all the individual images required for the study could not benefit for a rigorous application for the rule sets develop from the beginning of the research. By this, a rule set developed for one image was not applicable to the next image even though were for the same process (Möller, *et al.*, 2007). However, Clinton *et al.*, (2010) described the selection of scale parameter of a rule set as "a data exploration problem rather than an optimisation problem". Unfortunately, rule sets developed from a subset of the independent data with an accuracy of 85% in this study could not be used when applied to the whole image. This maybe either due to a poor representation of the subset or the inconsistency attributed to the trail-and-error of the segmentation process (Zhang et al., 2003). Hence, direct and continuous trail-and-error to a whole study site is the most suitable if more accurate segmented objects are to be achieved.

5.2. Image segmentation and validation

The accuracy assessment result of 74% from Geo-Eye and 79% from airborne LiDAR was based on a one-to-one matching of the digitised tree crowns to the automatically segmented tree crowns based on visual interpretation. The D-value obtained were respectively 66% (0.34) for Geo-Eye and 62% (0.377) for airborne LiDAR data. A *t-test* of both data sets proved that there was no significant difference in accuracy between the Geo-Eye image and the airborne LiDAR data using visual interpretation of the OBIA segmented tree crowns. Appendix 11 presents an assessment using a two-tail sample test with equal variance and the result of t-critical was greater than t-statistic ($t_{critical} = 1.98 > t_{stats} = -0.873$). Therefore, the null hypothesis there was a significant difference between the two data sets is rejected at 95% confidence interval. The 55 samples are the data for which the samples from one image are exactly the same to that of the other.

This implies segmentation of the tree crowns was better for the airborne LiDAR data compared to the Geo-Eye satellite image. The high value of the airborne LiDAR data can be attributed to fact that during the tree crown segmentation process, the data was truncated to eliminate all vegetation out of the threshold between 6 and 40 metres. Despite being conducted for trees outside forest within a tropical forest, the segmentation accuracy of this study was relatively high indicating that our spectral and shape characteristics introduced to the classifier were generated from segments that matched the tree crown objects. However, an attempt to improve on the degree of segmentation was not successful as much over-segmentation became more eminent.

This result is identical to what was obtained by Wang *et al.*, (2004) (75.6%) during their division of tree crown from non-tree crowns in a young created forest plantation in the north of British Columbia, Canada. Compared to the result obtained by Ke *et al.*, (2010) of a segmentation accuracy of 61.3% in a mixed forest of broad and needle leaf tree when region growing algorithm was employed, the result of this study seems to be better in both data sets.

The validation using the Java Topology Suite (JTS) and Geo-tools most probably minimises subjectivity of the visual interpreter during the segmentation process. Though the D value of 66% (0.34) for Geo-Eye and 62% (0.377) for LiDAR is less than that obtained in visual interpretation, the process is highly unbiased. Unfortunately, it is difficult to determine with precision if the discrepancy in the result is based on either a poor classifier or poor segmentation to the reference digitised tree crowns (Clinton, *et al.*, 2010). Applying the resulting image objects as sampling units makes it more complex as the size of any of the objects is considered as same (one unit) thereby resulting to the same effect with misclassification of either a small or large object (Radoux & Defourny, 2007). The result of this study maybe different based on the segmentation scales that are different from one another as explained earlier (*paragraph 5.1*). Hence, the segments developed from the different reference data sets cannot be directly compared except using point sampling units (Chubey, *et al.*, 2006).

5.3. Accuracy assessment of Canopy Height model (CHM) from airborne Lidar data

Tree height is a significant variable in the quantitative measurement of forest biomass and consequently carbon stock, growth and site productivity of a forest. The linear regression method had a mean estimator error ($h_{field} - h_{lidar}$) of roughly 26cm (RMSE = 13.59%) between the field measured tree height and airborne LiDAR tree height from local maxima. This error can be attributed to the error of the approximate fit of the regression line from the vertical layers returns and the measurements of the field tree height from the instruments used. This study was carried out in a mostly dominated deciduous trees outside forest that have got lots of branches that could have been detected by the LiDAR beams as other tree tops as shown in Figure 13 (Table 4 & Figure 2; B). However, the result from this study is better than that of Wang & Glenn, (2008) who had an error estimator of 51cm (RMSE ranged between 25 – 50%) in a predominantly pine tree dominated forest with just 79 tree samples in Idaho, USA. Moreover, the LiDAR mean tree height of this study (15.02m) compared to that of field observation (15.28m) confirms the result of Popescu et al., (2002) that the height underestimation is due to the fact that chances are high that the LiDAR beam misses the tree tops of the highest branch.

Compared to Andersen *et al.*, (2005), (R^2 = 0.98; RMSE = 1.3m) who worked in a pacific Northwest conifer forest, the R^2 = 0.912 and RMSE = 13.59% of this study is lower. The reason can be due to the difficulty in the identification of treetops for a mixed broadleaf forest compared to a species specific pine tree forest. Fortunately, this study is higher than the work of Hollaus *et al.*, (2006) whose R^2 ranged between 0.73 – 0.84% for species-specific Spruce and fir trees in a complex alpine forest. Unfortunately, none of their result was conducted neither in a mixed deciduous forest type nor in trees outside forest or generally carried out in a tropical forest environment that could have at least spelt a closer relationship.

5.4. Comparing DBH vs CPA

The non-linear polynomial coefficient of determination between the field measured CPA and the DBH ranged between 0.5 and 0.52 and were statistically significant ($p<0.005$) in all the data sets. The values of the R^2 were 0.520, 0.524, and 0.504 with RMSE 26%, 35.65% and 46.91% in airborne LiDAR, field measured data and VHR Geo-Eye satellite image respectively (Table 8). This result indicates that, R^2 from the LiDAR data was better than that from the Geo-Eye image with roughly half the RMSE percentage and within the range of results obtained by Anderson *et al.*, (2000). They obtained an R^2 that ranged between 0.37 and 0.8 for species-specific relationships in Akansa, USA. A functional relationship was reported between DBH and CPA in a deciduous broadleaf and coniferous forest based on field

measurements. But, he did not confirm the power sigmoid relationship though this study is based on a quadratic relationship. Compared to the Geo-Eye image, the good result of the airborne LiDAR can be attributed to the data truncation as this process eliminated the introduction of unwanted particles considered as noise (Maltamo *et al.*, 2004).

This result is lower than that of Avsar, (2004) who worked on Lebanon cedars in Turkey. He had an R^2=0.72 for CPA and DBH relationship based on a power model. The low result of this study can be attributed to trees species diversity as each tree species has specific behaviour corresponding to the different forest habitats (Baral *et al.*, 2009). There is also a usually practice of temporal pruning or lopping of the trees as either fodder for the cattle, fuel wood or timber by the farmers (Appendix 7; photos A, B & D). This has the advantage to allow sunlight penetrates into the rice fields to improve yield. Though care was taken that these types of trees should not be included in the sample, their biological recuperation is difficult to be differentiated with the limited time we had in the field.

5.5. Comparing CPAs

There was a strong linear relationship ($R^2 > 0.7$) between the field measured CPA and those from the segmentation of the remotely sensed data for trees outside forest. The result of the airborne LiDAR (R^2 = 0.74; RMSE = 38.24%; t = 3.13; $\alpha < 0.05$) is better than that for the VHR Geo-Eye satellite image (R^2 = 0.7327; RMSE = 41.18%; t = -1.125; $\alpha < 0.05$) and both of them were statistically significant. The discrepancy could be attributed to the shape and texture of the image object obtained from the segmentation process. Some individual tree crowns in the process were considered as double or more trees (26%) and roughly 3% of the measured trees were not segmented at all in the VHR Geo-Eye image (Figure 13). The 2 year time lapse in the acquisition of the Geo-Eye data and the field survey could also have affected the accuracy of the result as either the tree size or the shape of the tree crown could have increased in size (Song *et al.*, 2010) compared to that of airborne LiDAR that was just a couple of months. An alteration of the scale parameter from its origin of the subset produced a change in the segments that promoted the formation of larger tree crown making over-segmentation more conspicuous especially in the LiDAR data. The Geo-Eye image was taken at the beginning of leaf fall in Nepal that could have reduced the real structure of the crown shapes and making it difficult to differentiate the tree crowns and the undergrowth due to spectral reflectance. The Geo-Eye image seems to be taken either early in the morning or late in the evening. The sun angle made the shadows to be taller or larger than even the real trees thereby making segmentation difficult to obtain real crown objects.

5.6. Model development

Within a forest, an increase in tree girth does not necessarily increase the tree crown (Köhl, et al., 2006). In this perspective, a non-linear polynomial (quadratic) regression was used in the development of the mathematical model in both the airborne LiDAR and the VHR satellite Geo-Eye image since validation is based on the creation of a good testable hypothesis for a model in relation to the problem in course rather than a clear cut "true" model (Levins, 1966). Quadratic models also eliminate the possibility of having negative carbon stocks. The quadratic model was the best in the coefficient of determination with ($R^2 > 0.5$).

Linear relationships between DBH and crown diameter in a natural forest cannot be observed with trees that have a DBH greater than 40cm (Hemery, *et al.*, 2005). This is so because the rate of growth of the tree

girth and that of the tree crown are almost the same at the beginning, but the crown diameter will starts decreasing as the trees mature thereby taking a sigmoid shape of a normal growth curve. At maturity, the rate of growth is stabilised and as a result so too is the quantity of carbon stock in the plant until naturally die out.

The mathematical model developed for trees outside forest for carbon stock estimation has an R^2 of 0.5095 (RMSE = 42.24%) for Geo-Eye CPA, R^2 = 0.46 (RMSE = 41.29%) for LiDAR CPA, R^2 = 0.902 (RMSE = 14.24%) for airborne LiDAR tree height, and R^2 = 0.6898 (RMSE = 11.53%) for a multiple regression between the segmented CPA and tree height (CHM) obtained from the airborne LiDAR data (*confer 4.6*). The R^2 of the Geo-Eye and poor RMSE of 42.42% could be attributed to the pruning (*confer 5.4., paragraph 2*). Some of the trees were omitted during the segmentation process as can be seen in Figure 13. The high rate of commission error from the segmentation process by considering a single tree to have more than one crown is either due to the size of the crown from spectral reflectance (Appendix 7; D) or an abnormality of over- or under-segmentation resulting from the scale parameter (Clinton, *et al.*, 2010).

The prediction of carbon from CPA was seen to be best for the airborne LiDAR (R^2 = 0.46; RMSE = 41.29%) compared to the Geo-Eye that had a RMSE of 42.24% as explained above. This low prediction from CPA could be attributed to the segmentation process from which the image objects were subjected. Even with the inclusion of the watershed transformation and morphology for object re-shaping, the image objects of this study were difficult to be crown-like in shape. The activity of pruning usually practiced could have reduced the shape of the crowns resulting to over segmentation. Using the tree height independently from the LiDAR, R^2 was 0.902 (RMSE = 14.24%) that basically is due to the 3-D characteristic making it free from haze or clouds.

Integration of the LiDAR tree height and the CPA from the segmentation process in a multiple regression analysis gave an overall R^2 of 0.6898 with a RMSE of 11.53% (eq^n 11). Despite the low R^2 as compared to that from the CHM, the RMSE was conspicuously good as errors generated from either the determination of the tree height using local maximum filtering or the CPA from the segmentation process is compensated by the other. This however, introduces variations from the tree parameters thereby making multiple regression more significant statistically for trees outside forest.

5.7. Biomass and Carbon stock validation

Surprisingly, in validating the carbon stock model from the predicted and the observed calculations, the R^2 from Geo-Eye image with only CPA as a variable was the highest with 0.9701. This was followed by the LiDAR tree height (0.9037) and the multiple regression of tree height and CPA with 0.6898. Despite the high R^2 for the CPA from Geo-Eye model, the model is controlled by an outlier in the data set as the data is not equally distributed as seen on the graph (Figure 23a). Upon removal of the outlier, the R^2 was 0.362 that signifies a weak relationship between the observed and the predicted carbon based on the Geo-Eye CPA for trees outside forest. However, Appendix 7; D & F present a *Ficus spp.* tree whose crown diameter is more than the tree height. Situations of the nature could have contributed as an outlier that is difficult to be experience in a closed canopy forest because of tree branch intermingling (Lu, 2006) and direct competition for sunlight.

Considering the airborne LiDAR data, and comparing it to the Geo-Eye, the model validation for LiDAR height alone was very significant at R^2 = 0.9037. The sample data was more distributed around the mean.

Nevertheless, this was more visible in the multiple regression model of CPA and tree height from the airborne LiDAR data though with an R^2 of 0.6898 and RMSE of 11.53% as in eq^n 11 (Figure 22).

5.8. Biomass and Carbon stock estimation

Irrespective of the model used, a majority of the trees had carbon of <1000kg/tree and very few had carbon of >5000Kg/tree. From this study, tree height estimation had the highest carbon stock of 163.92 tons/ha. This result is comparatively smaller to that obtained in the Chitwan area for sparse vegetation of 140 tons carbon/ha (tC/ha) of total forest carbon density for the whole mid-altitude Kayarkhola watershed (ICIMOD, *et al.*, 2010). However, the result of this study is only based on trees outside forest while those for ICIMOD *et al.*, (2010) encloses everything in the watershed including sapling, herb, litter, soil and below ground carbon. But, the multiple regression model stands out as the best model in estimation of carbon stock for trees outside forest with a RMSE closest to zero.

5.9. Error in segmentation process

Despite working for trees outside forest, the shape of crowns was not as eminent as was expected in the Geo-Eye image. A fixed scale of 1:250 was applied during the on-screen digitisation process but the irregular patterns of the tree edges could have originated/introduced some errors of either over- or under-segmentation. At times, it is difficult to differentiate the limit of one tree and another tree or to separate 2 trees that have been recognised as a single tree from the image even after field data collection. However, this was limited for the airborne LiDAR data due to the truncation threshold that was introduced before the segmentation process.

Data for the study was acquired in November 2009 for the Geo-Eye which is the beginning of leaf fall in Nepal and most tropical countries and the field work was undertaken in September-October 2011. Leaf fall gives room for the understory to be conspicuously visible in the images thereby making tree identification difficult and fuzzy in the Geo-Eye image. In addition, the almost 2 years gap could have increased the size of the tree crowns (Song *et al.*, 2010) as some tropical hardwood trees have a yearly growth rate of 30.5cm. However, this could not be realised in the airborne LiDAR data as there was only 6 months difference between the time of data acquisition and the fieldwork survey.

Distinct boundaries between the tree crowns are difficult to be observed on the image. In addition, it seems difficult to clearly separate the reflectance of other vegetative structures like understory shrubs or grass/herbs of less than 5meters high for trees outside forest. An easy crispy identification is mostly obtained when natural boundaries of roads, rivers and tree hedges are used in separation of the rice farms.

However, the segmentation process of the airborne LiDAR data was less complicated with little errors. This was basically due to the truncation of the image during data pre-processing into rasterisation as all the noisy particles of less than 6m and more than 40m were eliminated during the process (Figure 4). Brightness of the objects segments and maximum pixel value were employed to obtain a distinct image objects as tree crowns.

5.9.1. Error from the allometric equation

Tropical forests has her uniqueness to comprise more than 300 different tree species in 1 hectare plot (Gentry, 1988) that makes it difficult for the application of species specific allometric equations in natural forest. However, this study had a total of 40 different species in the area occurring at different magnitude (Appendix 9). Variations in the structural characteristics (topography, age and soil type) of the forest

contribute as an uncertainty in the allometric equation. The allometric equation used in this study (*confer 3.8.1*) reduced the degree of error as it made use of wood specific density, DBH and tree height (Chave, et al., 2005). Wood specific density (ρ = 0.72) for lower slope mixed hardwood forest was used since our maximum altitude was 500m *asl*.

The derived coefficients in the allometric equation was confirmed as the main source of error by Kettering *et al.*, (2001) though her argument was on a non-linear power function in Sumatra, Indonesia. Hence, their usefulness is limited to the study area.

Similarly, errors may result during data collection from the measurements, sampling design and a poor representation of the study area especially with trees outside forest. Nonetheless, we expect a lesser error as the allometric equation employed for this study was developed for a tropical forest (Chave, *et al.*, 2005) and has been tested for carbon stock estimation in Nepal (Subedi, *et al.*, 2010).

5.10. Limitations of the study

The limitations of this study are:

- Differentiation of the pruned and un-pruned trees was not possible on the VHR Geo-Eye satellite image and even during field work it was difficult especially when the pruning period is more than 6 months. Though care was taken that the pruned trees should not be included in the sample, our result revealed some discrepancies in the characteristic behaviour commonly found for tree structural parameter in other studies (Hemery, *et al.*, 2005; Mora, *et a*l., 2010).
- Though species-specific allometric equation has been considered to produce good results for biomass and consequently carbon stock estimation, this study settled on the use of mixed allometric equation but making use of the wood specific density that is known to significantly contribute in models relating to AGB estimation (Chave, *et al.*, 2005).
- There was high off-nadir view angle in the Geo-Eye image that has been report to contribute significantly to the segmentation result. The tree crowns (CPAs) are difficult to be located by the softwares and this might have contributed enormously in the lower R^2 obtained in both images of the study despite the differences in sensors.
- The quality of the image was not the best as its acquisition was during the tree fall period. This helps to reduce the size of the tree crowns (Song *et al.*, 2010) and promotes the difficulty in separating the undergrowth from the tree tops.
- Figure 13 gives a presentation of some trees that were not segmented by the eCognition software during the segmentation process in Geo-Eye image. Such cases could have caused the less accuracy which is as a result of the software.

6. CONCLUSION AND RECOMMENDATIONS

Considering the complex nature of a tropical forest in its structure and function, the segmentation process remains promising and efficient in the identification of individual tree crowns. Though some of the trees outside forest could not be recognised in the segmentation process, a statistically acceptable R^2 that ranged from 0.5 to 0.9 for both data sets between carbon, tree height and CPA spells a consistency of the Definiens technique for carbon stock estimation with a validation from the field data. From the objectives of the study, the following conclusions were arrived:

6.1. Conclusions

- What is the difference in accuracy segmentation using VHR Geo-eye satellite image and airborne LiDAR data for trees outside forest?

The result of both data sets produced a good result using visual interpretation with an accuracy assessment greater than 70% (Geo-Eye = 74% & LiDAR = 79%) in the use OBIA in mixed deciduous dominated trees outside forest in a tropical milieu. In comparing the CPAs of both data sets in a *t-test*, it was realised that there was no significant difference in accuracy between the Geo-Eye image and the airborne LiDAR data using visual interpretation of the OBIA segmented tree crowns ($t_{critical} = 1.98 > t_{stats} = -0.873$). Therefore, the null hypothesis there was a significant difference between the two data sets is rejected at 95% confidence interval.

- How strong is the relationship between forest stand parameters i.e. CPA and height extracted from remotely sensed data and field data for individual trees outside forest?

Generally, there was a strong relationship ($R^2>0.7$) between the field measured forest stand parameters and that obtained from remotely sensed data. The strongest relationship ($R^2 = 0.912$) was between the tree height obtained from the airborne LiDAR and that of field measurement. R^2 for field CPA and Geo-Eye CPA was 0.733 (RMSE=41.18) while that of airborne LiDAR was 0.743 (RMSE=38.24%). These differences could be attributed to off-nadir view angle, time of image acquisition (*confer 5.5*).

- What is the quantity of carbon stock in trees outside forest in the Kayarkhola watershed, Nepal?

Carbon stock for trees outside forest was computed based on the 4 independent models. The quantity of carbon stored by the trees from a quadratic regression model of tree heights of the airborne LiDAR was the most impressive (roughly 163 tons/ha). A multiple regression analysis was employed between the parameters (CPA & tree height) obtained from the airborne LiDAR data.

6.2. Recommendations

The role for trees outside forest as fuel wood and fodder makes it a powerful "leakage" to the well protected surrounding community forests. Their protection will promote conservation priorities of the Kayarkhola watershed which can bring in more benefits in terms of its carbon credits to the CFUGs and the Forestry Department as a whole.

The same study should be repeated with a stratified random sampling of crown sizes for a uniform distribution of the data set. This may possibly improve the outcome of the result where the data set would be evenly distributed within the study area.

The validation results of this study from both data sets were highly significant for the field measured and the remotely sensed data (R^2>0.7) and as such can be recommended for future use in biomass and carbon estimations.

The use of a general allometric equation due to the quantity of data available since the field data couldn't have been good for species specific allometric relationships. It will be of significance for more data to be collected or the sample study area increased so that species wise allometric equations of CPA and tree height can be employed for a comparative study here described.

As of now, the result of this study is valid only for trees whose diameter at breast height is greater than 10cm and height more than 6m except an additional study is accompanied this present one.

LIST OF REFERENCES

Alves, L. F., & Santos, F. A. M. (2002). Tree allometry and crown shape of four tree species in Atlantic rain forest, south-east Brazil. *Journal of tropical ecology, 18*(2), 245-260.

Andersen, H.-E., McGaughey, R. J., & Reutebuch, S. E. (2005). Estimating forest canopy fuel parameters using LIDAR data. *Remote Sensing of Environment, 94*, 441-449.

Anderson, S. C., Kupfer, J. A., Wilson, R. R., & Cooper, R. J. (2000). Estimating forest crown area removed by selection cutting: a linked regression-GIS approach based on stump diameters. *Forest Ecology and Management, 137*(1–3), 171-177.

ANSAB. (2010). *Forest Carbon Stock Measurement: Guidelines for measuring carbon stocks in community-managed forests* (1st ed.). Kathmandu, Nepal: ANSAB, FECOFUN, ICIMOD.

Asner, G. P. (2009). Tropical forest carbon assessment: integrating satellite and airborne mapping approaches. *Environmental Research Letters, 4*(3), 034009.

Avsar, M. D. (2004). The Relationships between Diameter at Breast Height, Tree Height and Crown Diameter in Lebanon Cedars (Cedrus libani A. Rich.) of the Yavsan Mountain, Kahramanmaras, Turkey. *Journal of Biological Sciences, 4*(4), 437-440.

Baatz, M., & Schäpe, A. (2000). *Multiresolution Segmentation: an optimization approach for high quality multi-scale image segmentation*. Paper presented at the 2nd Intl. Symposium. Operationalization of Remote Sensing, 16-20 August, ITC, NL, Wichmann.

Baral, S. K., Malla, R., & Ranabhat, S. (2009). Above-ground carbon stock assessment in different forest types of Nepal. *Banko Janakari, 19*(2), 10-14.

Basuki, T. M., van Laake, P. E., Skidmore, A. K., & Hussin, Y. A. (2009). Allometric equations for estimating the above-ground biomass in tropical lowland Dipterocarp forests. *Forest Ecology and Management, 257*(8), 1684-1694.

Benz, U. C., Hofmann, P., Willhauck, G., Lingenfelder, I., & Heynen, M. (2004). Multi-resolution, object-oriented fuzzy analysis of remote sensing data for GIS-ready information. *Isprs Journal of Photogrammetry and Remote Sensing, 58*(3-4), 239-258.

Blair, J. B., & Hofton, M. A. (1999). Modeling Laser Altimeter Return Waveforms Over Complex Vegetation Using High-Resolution Elevation Data *Geophysical Research Letters, 26*(16), 2509.

Blaschke, T. (2010). Object based image analysis for remote sensing. *Isprs Journal of Photogrammetry and Remote Sensing, 65*(1), 2-16.

Bortolot, Z. J., & Wynne, R. H. (2005). Estimating forest biomass using small footprint LiDAR data: An individual tree-based approach that incorporates training data. *Isprs Journal of Photogrammetry and Remote Sensing, 59*(6), 342-360.

Brown, S. (2002). Measuring carbon in forests: current status and future challenges. *Environmental Pollution, 116*(3), 363-372.

Brown, S., Gillespie, A. J. R., & Lugo, A. E. (1989). Biomass Estimation Methods for Tropical Forests with Applications to Forest Inventory Data. *Forest Science, 35*(4), 881-902.

Brown, S. L., & Schroeder, P. E. (1999). Spatial Patterns of Aboveground Production and Mortality of Woody Biomass for Eastern U.S. Forests. *Ecological Applications, 9*(3), 968-980.

Chave, J., Andalo, C., Brown, S., Cairns, M., Chambers, J. Q., Eamus, D., Fölster, H., Fromard, F., Higuchi, N., Kira, T., Lescure, J.P., Nelson, B.W., Ogawa, H., Puig, H., Riéra, B. & Yamakura, T. (2005). Tree allometry and improved estimation of carbon stocks and balance in tropical forests. *Oecologia, 145*(1), 87-99.

Chen, L.-C., Teo, T.-A., Shao, Y.-C., Lai, Y.-C., & Rau, J.-Y. (2003). Fusion of LiDAR data and Optical imagery for building models *Building, 35*(B4), 2-7.

Chubey, M. S., Franklin, S. E., & Wulder, M. A. (2006). Object-based analysis of Ikonos-2 imagery for extraction of forest inventory parameters *Photogrammetric engineering and remote sensing, 72*(4), 383.

Clinton, N., Holt, A., Scarborough, J., Yan, L., & Gong, P. (2010). Accuracy Assessment Measures for Object-based Image Segmentation Goodness. *Photogrammetric Engineering & Remote Sensing, 76*(3), 289–299.

Drake, J. B., Knox, R. G., Dubayah, R. O., Clark, D. B., Condit, R., Blair, J. B., & Hofton, M. (2003). Above-ground biomass estimation in closed canopy Neotropical forests using lidar remote sensing: factors affecting the generality of relationships. *Global Ecology and Biogeography, 12*(2), 147-159.

FAO. (2002). *Trees outside forests: towards a better awareness*. Rome, Italy: FAO.

FAO. (2010). *Global Forest Resources Assessment 2010: Main Report. FAO Forestry Paper 163*. Rome, Italy: Food and Agriculture Organization of the UN.

Foody, G. M., Boyd, D. S., & Cutler, M. E. J. (2003). Predictive relations of tropical forest biomass from Landsat TM data and their transferability between regions. *Remote Sensing of Environment, 85*(4), 463-474.

Fortin, M. J., Olson, R. J., Ferson, S., Iverson, L., Hunsaker, C., Edwards, G., Levine, D., Butera, K. & Klemas, V. (2000). Issues related to the detection of boundaries. *Landscape Ecology, 15*(5), 453-466.

Gatziolis, D., Fried, J. S., & Monleon, V. S. (2010). Challenges to Estimating Tree Height via LiDAR in Closed-Canopy Forests: A Parable from Western Oregon. *Forest Science, 56*(2), 139-155.

Gautam, B., & Kandel, P. (2010). Working paper on LiDAR mapping in Nepal. Submitted to the Ministry of Forests and Soil Conservation on 26 March 2010. Retrieved 15 July 2010, from http://www.forestrynepal.org/publications/article/4771

Gentry, A. H. (1988). Tree species richness of upper Amazonian forests. *Proceedings of the National Academy of Sciences, 85*(1), 156-159.

Gibbs, H. K., Brown, S., Niles, J. O., & Foley, J. A. (2007). Monitoring and estimating tropical forest carbon stocks: making REDD a reality. *Environmental Research Letters, 2*(4), 045023.

Goetz, S., Baccini, A., Laporte, N., Johns, T., Walker, W., Kellndorfer, J., Houghton, R. & Sun, M. (2009). Mapping and monitoring carbon stocks with satellite observations: a comparison of methods. *Carbon Balance and Management, 4*(1), 1-7.

Gougeon, F. (1995). A Crown-Following Approach to the Automatic Delineation of Individual Tree Crowns in High Spatial Resolution Aerial Images. *Canadian Journal of Remote Sensing, 21*(3), 274-284.

Gougeon, F. A., Cormier, R., Labrecque, P., Cole, B., Pitt, D. G., & Leckie, D. G. (2003). *Tree crown (ITC) delineation on Ikonos and QuickBird imagery: the Cockburn Island study* Paper presented at the 25th Canadian Symposium on Remote Sensing.

Hay, G. J., Blaschke, T., Marceau, D. J., & Bouchard, A. (2003). A comparison of three image-object methods for the multiscale analysis of landscape structure. *ISPRS Journal of Photogrammetry and Remote Sensing 57*(5-6), 327-345.

Hemery, G. E., Savill, P. S., & Pryor, S. N. (2005). Applications of the crown diameter-stem diameter relationship for different species of broadleaved trees. *Forest Ecology and Management, 215*(1-3), 285-294.

Herrera, F. B. (2003). *Classification and modeling of trees outside forest in Central American landscapes by combining remotely sensed data and GIS*. Unpublished Ph.D Dissertation, University of Frieburg, Frieburg, Germany.

Hese, S., Lucht, W., Schmullius, C., Barnsley, M., Dubayah, R., Knorr, D., Neumann, K., Riedel, T. & Schroter, K. (2005). Global biomass mapping for an improved understanding of the CO_2 balance--the Earth observation mission Carbon-3D. *Remote Sensing of Environment, 94*(1), 94-104.

Hollaus, M., Wagner, W., Eberhöfer, C., & Karel, W. (2006). Accuracy of large-scale canopy heights derived from LiDAR data under operational constraints in a complex alpine environment. *Isprs Journal of Photogrammetry and Remote Sensing, 60*(5), 323-338.

Holmgren, P., & Thuresson, T. (1998). Satellite remote sensing for forestry planning A review. *Scandinavian Journal of Forest Research, 13*(1), 90-110.

Houghton, J. T., Callander, B. A., & Varney, S. K. (Eds.). (1992). *Climate Change 1992: The Supplemantary Report to the IPCC Scientific Assessment*. Cambridge, UK: Intergovernmental Panel on Climate Change, Cambridge University Press.

Houghton, R. A., Lawrence, K. T., Hackler, J. L., & Brown, S. (2001). The spatial distribution of forest biomass in the Brazilian Amazon: a comparison of estimates. *Global Change Biology, 7*(7), 731-746.

Hyyppa, J., Kelle, O., Lehikoinen, M., & Inkinen, M. (2001). A segmentation-based method to retrieve stem volume estimates from 3-D tree height models produced by laser scanners. *Geoscience and Remote Sensing, IEEE Transactions on, 39*(5), 969-975.

ICIMOD, ANSAB, & FECOFUN. (2010). *Report on forest carbon stocks in Ludikhola, Kayarkhola and Charnawati Watersheds of Nepal:* . Kathmandu, Nepal: ICIMOD, ANSAB, FECOFUN.

IPCC. (2006). 2006 IPCC Guidelines for National Greenhouse Gas Inventories. In: H. S. Eggleston, L. Buendia, K. Miwa, T. Ngara & K. Tanabe (Eds.), *Volume 4 Agriculture, Forestry and Other Land Use*. Hayama, Japan: Institute for Global Environmental Strategies (IGES).

IPCC. (2007). Climate Change 2007: The Physical Science Basis. Contribution of Working Group I to the Fourth Assessment. In S. Solomon, D. Qin, M. Manning, Z. Chen, M. K. Marquis, B. Averyt, M. Tignor & H. L. Miller (Eds.), *Report of the Intergovernmental Panel on Climate Change* (pp. 996). Cambridge, United Kingdom & New York, NY, USA: Cambridge University Press.

JTS. (2012). GeoTools 8.0 - M3 User Guide. Retrieved 31 Jan 2012, from http://docs.geotools.org/latest/userguide/library/jts/index.html

Kale, M., Ravan, S., Roy, P., & Singh, S. (2009). Patterns of carbon sequestration in forests of western ghats and study of applicability of remote sensing in generating carbon credits through afforestation/reforestation. *Journal of the Indian Society of Remote Sensing, 37*(3), 457-471.

Ke, Y., Quackenbush, L. J., & Im, J. (2010). Synergistic use of QuickBird multispectral imagery and LIDAR data for object-based forest species classification. *Remote Sensing of Environment, 114*(6), 1141-1154.

Ketterings, Q. M., Coe, R., van Noordwijk, M., Ambagau', Y., & Palm, C. A. (2001). Reducing uncertainty in the use of allometric biomass equations for predicting above-ground tree biomass in mixed secondary forests. *Forest Ecology and Management, 146*(1–3), 199-209.

Kim, S., McGaughey, R. J., Andersen, H.-E., & Schreuder, G. (2009). Tree species differentiation using intensity data derived from leaf-on and leaf-off airborne laser scanner data. *Remote Sensing of Environment, 113*(8), 1575-1586.

Köhl, M., Magnussen, S., & Marchetti, M. (2006). Sampling in Forest Surveys *Sampling Methods, Remote Sensing and GIS Multiresource Forest Inventory* (pp. 71-196): Springer Berlin Heidelberg.

Kumar, R. (2005). *Research Methodology: A Step-By-Step Guide for Beginners*. London, UK; California, USA; New Delhi, India: SAGE Publications Inc.

Lefsky, M. A., Cohen, W. B., Parker, G. G., & Harding, D. J. (2002a). Lidar Remote Sensing for Ecosystem Studies. *BioScience, 52*(1), 19-30.

Levins, R. (1966). "The Strategy of Model Building in Population Biology". *American Scientist, 54*, 421-431.

Li, X., & Strahler, A. H. (1985). Geometric-Optical Modeling of a Conifer Forest Canopy. *Geoscience and Remote Sensing, IEEE Transactions on, GE-23*(5), 705-721.

Lim, K. P., Treitz, P., Wulder, M. A., St-Onge, B. A., & Flood, M. (2003). LiDAR remote sensing of forest structure. *Progress in Physical Geography, 27*(1), 88-106.

Lohmann, P. (2002). *Segmentation and filtering of laser scanner digital surface models* Paper presented at the IAPRS, Xi' an, 20-23, Aug, 2002, pp311-316.

Lu, D. (2005). Aboveground biomass estimation using Landsat TM data in the Brazilian Amazon. *International Journal of Remote Sensing, 26*(12), 2509-2525.

Lu, D. (2006). The potential and challenge of remote sensing-based biomass estimation. *International Journal of Remote Sensing, 27*(7), 1297-1328.

Lugo, A. E., & Brown, S. (1986). Steady state terrestrial ecosystems and the global carbon cycle. *Plant Ecology, 68*(2), 83-90.

MacDicken, K. G. (1997). *A Guide to Monitoring Carbon Storage in Forestry and Agroforestry Projects*. Winrock: Winrock International Institute for Agricultural Development.

Maltamo, M., Eerikäinen, K., Pitkänen, J., Hyyppä, J., & Vehmas, M. (2004). Estimation of timber volume and stem density based on scanning laser altimetry and expected tree size distribution functions. *Remote Sensing of Environment, 90*(3), 319-330.

Möller, M., Lymburner, L., & Volk, M. (2007). The comparison index: A tool for assessing the accuracy of image segmentation. *International Journal of Applied Earth Observation and Geoinformation, 9*(3), 311-321.

Mora, B., Wulder, M. A., & White, J. C. (2010). Segment-constrained regression tree estimation of forest stand height from very high spatial resolution panchromatic imagery over a boreal environment. *Remote Sensing of Environment, 114*(11), 2474-2484.

Neteler, M., & Mitasova, H. (2008). Satellite Image Processing: . In M. Neteler & H. Mitasova (Eds.), *Open Source GIS: A Grass GIS Approach* (Third ed., pp. 405). New York, USA: Springer.

Pan, Y., Birdsey, R. A., Fang, J., Houghton, R., Kauppi, P. E., Kurz, W. A., Phillips, O. L., Shvdenko, A., Lewis, S. L., Canadell, J. G., Ciais, P., Jackson, R. B., Pacala, S., McGuire, A. D., Piao, S., Rautiainen, A., Sitch, S. & Hayes, D. (2011). A Large and Persistent Carbon Sink in the World's Forests. *Science*.

Patenaude, G., Milne, R., & Dawson, T. P. (2005). Synthesis of remote sensing approaches for forest carbon estimation: reporting to the Kyoto Protocol. *Environmental Science & Policy, 8*(2), 161-178.

Pohl, C., & Van Genderen, J. L. (1998). Multisensor image fusion in remote sensing: concepts, methods and applications. *International Journal of Remote Sensing 19*(5), 823-854.

Popescu, S. C. (2007). Estimating biomass of individual pine trees using airborne lidar. *Biomass and Bioenergy, 31*(9), 646-655.

Popescu, S. C., Wynne, R. H., & Nelson, R. F. (2002). Estimating plot-level tree heights with lidar: local filtering with a canopy-height based variable window size. *Computers and Electronics in Agriculture, 37*(1-3), 71-95.

Radoux, J., & Defourny, P. (2007). A quantitative assessment of boundaries in automated forest stand delineation using very high resolution imagery. *Remote Sensing of Environment, 110*(4), 468-475.

Rosenqvist, Å., Milne, A., Lucas, R., Imhoff, M., & Dobson, C. (2003). A review of remote sensing technology in support of the Kyoto Protocol. *Environmental Science & Policy, 6*(5), 441-455.

Song, C. (2007). Estimating tree crown size with spatial information of high resolution optical remotely sensed imagery. *International Journal of Remote Sensing, 28*(15), 3305-3322.

Song, C., Dickinson, M. B., Su, L., Zhang, S., & Yaussey, D. (2010). Estimating average tree crown size using spatial information from Ikonos and QuickBird images: Across-sensor and across-site comparisons. *Remote Sensing of Environment, 114*(5), 1099-1107.

Subedi, B. P., Pandey, S. S., Pandey, A., Rana, E. B., Bhattarai, S., Banskota, T. R., Charmarkar, S. & Tamrakar, R. (2010). *Forest Carbon Stock Measurement: Guidelines for measuring carbon stocks in community-managed forests.* (first ed.). Kathmandu, Nepal: Asia Network for Sustainable Agriculture and Bioresources (ANSAB), FECOFUN, ICIMOD.

Tans, P. P., Fung, I. Y., & Takahashi, T. (1990). Observational constraints on the global atmospheric carbon dioxide budget. *Science, 247*, 1431-1438.

UN-REDD. (2008). *United Nations Collaborative Programme on Reducing Emissions from Deforestation and Forest Degradation in Developing Countries (UN-REDD): Framework document*. Rome, Italy: FAO, UNEP, UNDP.

Verwijst, T., & Telenius, B. (1999). Biomass estimation procedures in short rotation forestry. *Forest Ecology and Management, 121*(1-2), 137-146.

Wang, C., & Glenn, N. F. (2008). A linear regression method for tree canopy height estimation using airborne lidar data. *Canadian Journal of Remote Sensing, 34*(S2), S217-S227.

Wang, H., Hall, C. A. S., Scatena, F. N., Fetcher, N., & Wu, W. (2003). Modeling the spatial and temporal variability in climate and primary productivity across the Luquillo Mountains, Puerto Rico. *Forest Ecology and Management, 179*(1-3), 69-94.

Wang, L., Gong, P., & Biging, G. S. (2004). Individual Tree-Crown Delineation and Treetop Detection in High-Spatial-Resolution Aerial Imagery. *Photogrammetric Engineering & Remote Sensing, 70*(3), 351-357.

Wang, S., Chen, J. M., Ju, W. M., Feng, X., Chen, M., Chen, P., & Yu, G. (2007). Carbon sinks and sources in China's forests during 1901-2001. *Journal of Environmental Management, 85*(3), 524-537.

Weidner, U. (2008). Contribution to the assessment of segmentation quality for remote sensing applications. *The International Archives of the Photogrammetry, Remote Sensing and Spatial Information Sciences, XXXVII*(B7), 479 - 484.

Westlake, D. F. (1963). Comparisons for plant productivity. *Biological Review, 38*, 385-425.

Woodcock, C. E., Collins, J. B., Jakabhazy, V. D., Xiaowen, L., Macomber, S. A., & Yecheng, W. (1997). Inversion of the Li-Strahler canopy reflectance model for mapping forest structure. *Geoscience and Remote Sensing, IEEE Transactions on, 35*(2), 405-414.

Wulder, M. (1998). Optical remote-sensing techniques for the assessment of forest inventory and biophysical parameters *Progress in Physical Geography, 22*(4), 449-476.

APPENDICES

Appendix 1: Tree species encountered outside forest, Kayarkhola watershed, Chitwan, Nepal

	Local names	**Scientific names**	**Plant family**
1	Asna/ saj	*Terminalia tomentosa*	Combretaceae
2	Badahar	*Articarpus lakoocha*	Moraceae
3	Barro	*Terminalia bellerica*	Combretaceae
4	Bayer	*Zizyphus jujube*	Rhamnaceae
5	Bel	*Aegle marmelos*	Rutaceae
6	Bakaino	*Melia azedarach*	Meliaceae
7	Botdhayero	*Lagerstromia parviflora*	Meliaceae
8	Chilaune	*Schima wallichiana*	Theaceae
9	Chiuri	*Madhuca buttyracea*	Sapotaceae
10	Chiple	*Villebrunnea frutescens*	Urticaceae
11	Dabdabe	*Daphne papyracea*	Thymelaeaceae
12	Dumare	*Ficus glomerata*	Moraceae
13	Pipal	*Ficus religiosa*	Moraceae
14	Ficus	*Ficus bengalensis*	Moraceae
14	Kadam	*Anthocephalus cadamba*	Rubiaceae
15	Kadu	*Cynecardia odorata*	Flacourtiaceae
16	Khanyo	*Ficus semicordata*	Moraceae
17	Khanyu	*Ficus cunia*	Moraceae
18	Kabro	*Ficus lacer*	Moraceae
19	Khari	*Celtis australis*	Ulmaceae
20	Indra jow	*Holarrhena antidysenterica*	Apolynaceae
21	Khokila	*n/a*	n/a
22	Kimba	*Morus alba*	Moraceae
23	Kharseto	*Ficus hispida*	Moraceae
24	Kadhero	*Litsea polyantha*	Lauraceae
25	Lapsi	*Choerospondias axillaris*	Anarcardiaceae
26	Lychee	*Litchi chinensis*	Sapindaceae
27	Amp	*Mangifera indica*	Anarcardiaceae
28	Chatiwan	*Alstonia scholaris*	n/a
29	Nebharo	*Ficus rexburghii*	Moraceae
30	Kraysi	*Priotropis cytisoides*	Moraceae
31	Sal	*Shorea robusta*	
32	Singane	*n/a*	n/a
33	Simal	*Bombax ceiba*	Bombacaceae
34	Siris	*Albizia procera*	Leguiminosae
35	Sissoo	*Dalbergia sissoo*	Leguiminosae
36	Taki	*Bauhinia purpurea*	Leguminosae
37	Teak	*Techtonia grandis*	Verbanaceae
38	Bheller	*n/a*	n/a
39	Jamun	*Syzigium cumini*	Myrtaceae

Appendix 2: List field equipments and software and their functions

	Equipment	**Function**
1	iPAQ and GPS	Navigation
2	Suunto compass	Orientation
3	Diameter tape	Diameter measurement
4	Measuring tape (30m)	Length measurement
5	Haga altimeter	Tree height measurement
6	Slope meter	Slope measurement
7	Data sheets	Collection of field data
	Softwares	
8	ArcGIS 10	GIS analysis
9	ERDAS 2011 & ENVI 4.8	Image processing and remote sensing applications
10	eCognition Developer 8	Tree crown delineation and classification (OBIA)
11	Lastools	Analysis of LiDAR data
12	Quick Terrain Modeller	Lidar analysis
13	R software, Excel 2010	Statistical analysis
14	Microsoft office & Endnote	Thesis writing

Appendix 3: Table of metadata of airborne LiDAR data

Customer	Forest Resource Assessment in Nepal, Ministry of Forests and Soil Conservation
Date Flown	20110316 / 20110328 / 20110401 / 20110402
Times of collection (UTC)	02:45 – 08:20 / 03:46 – 05:00 / 04:01 – 05:45 / 03:31 – 05:30
Date Processed	20110530
Projection	UTM
Datum	WGS84
Files included	ASPRS LAS v. 1.2 - 3002 nos.(IC01.las to IV300.las)
Aerial Platform	Helicopter (9N-AIW)
Flying altitude	2200 m AGL
Flying speed	80 knots
Sensor pulse rate	52.9 khz
Sensor Scan speed	20.4 lines/second
Nominal outgoing pulse density @ground level	Average: 0.8 points per square meter
Scan FOW half-angle	20 degrees
Swath @ ground level	1601.47 m
Point spacing	max 1.88 m across, max 2.02 m down
Laser beam setting (Optech)	-
Beam footprint @ ground level	50 cm
Gap file name	No gaps
Tile index file name	tile index_Block_icomod.dgn
Comments	

Appendix 4: Table of the metadata of ortho-photo

Image type	RGB image optimized for automatic interpretation.
Format	GeoTIFF with tfw
Compression	Image files non-compressed TIFF.
Source	From digital sensor
View angle	Nadir –looking
Collection procedure	Image files will be collected during the LiDAR acquisition.
Resolution	0.45 m at 2500 agl altitude
Orthorectification	The image has to be ortho-rectified to 1 m horizontal precision over the LiDAR.
Bands	The image files contain three bands: R, G, and B.
NIR width (approximate)	830 - 1100nm
R width (app.)	610 - 660nm
G width (app.)	530 - 590nm
B width (app.)	not available.
Color Balancing	The image files are color- balanced over the project area. Preferably, satellite image is used in color balancing as a reference.
Opening angles	Max 16 degrees off-nadir in the final product. (Wider angle can be used to cover overlaps if necessary)
Flight line direction	According to the LiDAR flight plan.
Weather conditions	Preferably they are obtained with clear weather.
Sun angle	Sun angle must not be less than 40 degrees and, preferably, not more than 80 degrees above horizon during the collect.
Clouds	No more than 3% of cloud cover or cloud shadows are accepted. If clouds or cloud shadows exist, a polygon shape file or DGN has to be delivered to show all clouded areas. If more clouds are received, a discussion and production unit's confirmation about the data usability is needed.
Season	All trees have to be under full leaf cover and green. In Nepal the photographic months are from October to March. This will be discussed with the clients and the time period will be selected.
Projection	UTM zone 45N
Band registration error	Maximum band-to-band dislocation 0.3 pixels
Horizontal location error	Max +/-1m
Tiling	Images are tiled to 12Mb each.
Image Tile index	Ortho_tile index_Block_Icimod

Appendix 5: Java intersector for airborne LiDAR segmentation

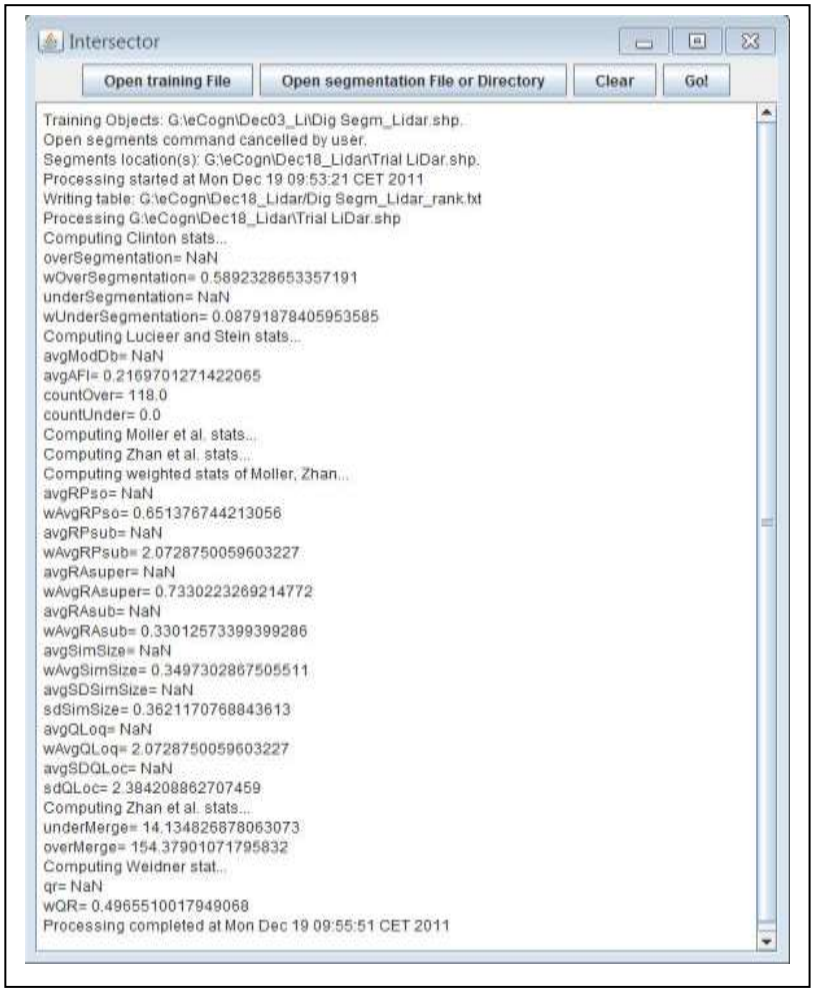

Appendix 6: Java intersector for Geo-Eye segmentation

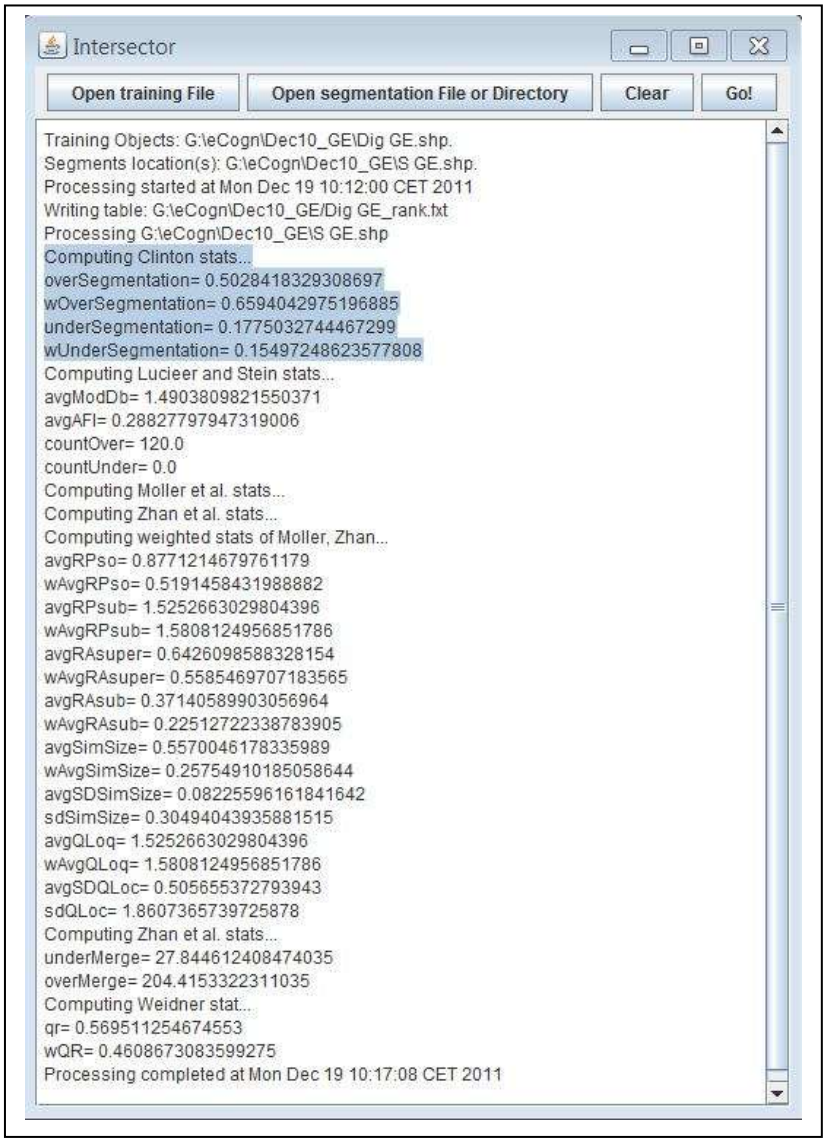

Appendix 7: Pruned and normal trees displayed

A: *pruned tree*

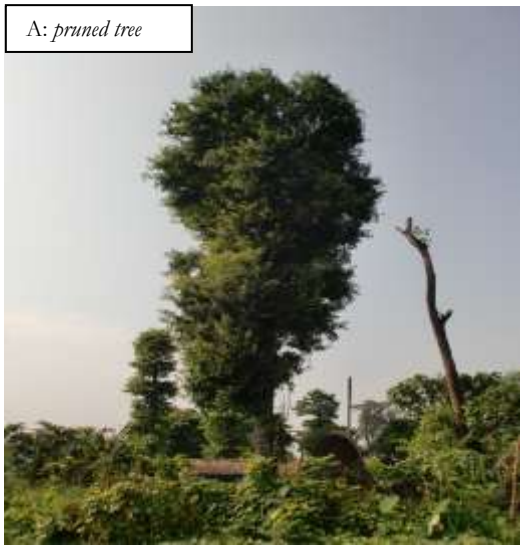

B: *pruned tree*

C: *normal tree*

D: *pruned tree*

E: *normal tree*

F: *normal tree*

Appendix 8: Descriptive statistics of the 3 data sets

	Field CPA (m^2)	Geo-Eye CPA (m^2)	Lidar CPA (m^2)
Mean CPA (m^2)	70.23	37.395	51.52
Standard Error	3.396	3.31	3.31
Standard Deviation	52.51	37.54	39.44
Minimum	7.07	6	10
Maximum	397.41	283	329
Count	238	129	142
Confidence level	6.88	6.54	6.543

Appendix 9: Distribution of tree species for trees outside forest

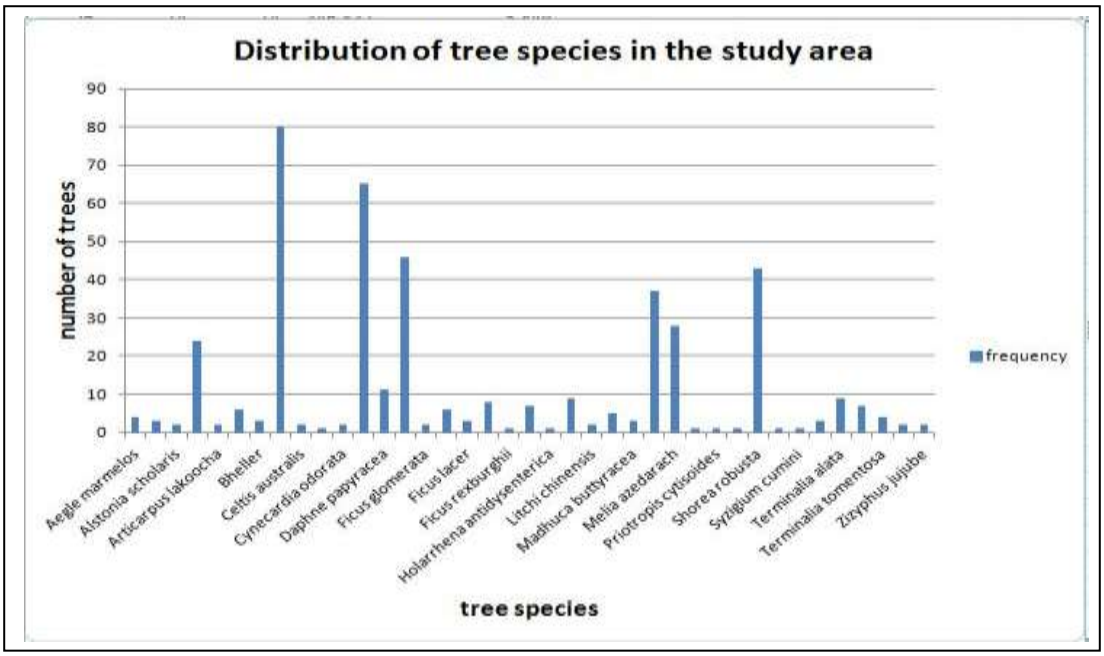

Appendix 10: Summary of field measured data

	DBH	Tree height	CPA
Minimum	10	6	3
1st quartile	25	11	7
Median	32	14	8
Mean	40.77	15.27	8.634
3rd quartile	50	18	10
Maximum	138	33	24

Appendix 11: Result of the t-test

t-Test: Two-Sample Assuming Equal Variances

	Geo-Eye	*LiDAR*
Mean	45,32727273	52,65455
Variance	1620,63165	2252,156
Observations	55	55
Pooled Variance	1936,393939	
Hypothesized Mean Difference	0	
df	108	
t Stat	-0,873196218	
P(T<=t) two-tail	0,384493495	
t Critical two-tail	1,982173424	